ASC Report No. 14/2017

Practical splitting methods for the adaptive integration of nonlinear evolution equations. Part II: Comparison of local error estimation and step-selection strategies for nonlinear Schrödinger and wave equations

W. Auzinger, I. Brezinova, H. Hofstätter, O. Koch, M. Quell

Institute for Analysis and Scientific Computing
Vienna University of Technology — TU Wien
www.asc.tuwien.ac.at ISBN 978-3-902627-00-1

Most recent ASC Reports

13/2017 *L. Banjai, J.M. Melenk, R.H. Nochetto, E. Otarola, A. Salgado, and C. Schwab*
Tensor FEM for spectral fractional diffusion

12/2017 *S. Börm, C. Börst, J.M. Melenk*
An analysis of a butterfly algorithm

11/2017 *X. Chen and A. Jüngel*
A note on the uniqueness of weak solutions to a class of cross-diffusion styles

10/2017 *A. Gerstenmayer and A. Jüngel*
Analysis of a degenerate parabolic cross-diffusion system for ion transport

09/2017 *M. Löhndorf and J.M. Melenk*
On thin plate spline interpolation

08/2017 *A. Sokolova and H. Woracek*
Termination in Convex Sets of Distrubtions

07/2017 *R. Pruckner*
Density of the spectrum of Jacobi matrices with power asymptotics

06/2017 *T. Führer and D. Praetorius*
A linear Uzawa-type solver for nonlinear transmission problems

05/2017 *A. Jüngel and S. Schuchnigg*
A discrete Bakry-Emery method and its application to the porous-medium equation

04/2017 *M. Bulicek, M. Pokorny, and N. Zamponi*
Existence analysis for incompressible fluid model of electrically charged chemically reacting and heat conducting mixtures

Institute for Analysis and Scientific Computing
Vienna University of Technology
Wiedner Hauptstraße 8–10
1040 Wien, Austria

E-Mail: admin@asc.tuwien.ac.at
WWW: http://www.asc.tuwien.ac.at
FAX: +43-1-58801-10196

ISBN 978-3-902627-00-1

Practical splitting methods for the adaptive integration of nonlinear evolution equations. Part II: Comparisons of local error estimation and step-selection strategies for nonlinear Schrödinger and wave equations

Winfried Auzinger[a], Iva Brezinova[b], Harald Hofstätter[b], Othmar Koch[c], Michael Quell[a]

[a] *Institute for Analysis and Scientific Computing, Vienna University of Technology, Wiedner Hauptstraße 8-10, A–1040 Wien, Austria.*
[b] *Institute for Theoretical Physics, Vienna University of Technology, Wiedner Hauptstraße 8-10, A–1040 Wien, Austria.*
[c] *Institut für Mathematik, Universität Wien, Oskar-Morgensternplatz 1, A-1090 Wien, Austria.*

Abstract

We compare the practical performance of adaptive splitting methods for the solution of nonlinear Schrödinger equations. Different methods for local error estimation are assessed with respect to their accuracy and efficiency in conjunction with promising strategies for step-size adaptation. The numerical comparisons comprise the cubic nonlinear Schrödinger equation with a blow-up solution, systems of coupled nonlinear Schrödinger equations, a rotational and a Gross–Pitaevskii equation under a highly oscillatory potential inducing wave chaos, and a quantum control model with a time-dependent potential. Finally, for nonlinear wave equations we demonstrate the enhanced computational stability ensuing from adaptive step selection strategies close to the border mandated by the CFL condition.

Keywords: Nonlinear Schrödinger equations, splitting methods, local error estimators, adaptive step-size selection, embedded methods, defect–based

Email addresses: w.auzinger@tuwien.ac.at (Winfried Auzinger), iva.brezinova@tuwien.ac.at (Iva Brezinova), hofi@harald-hofstaetter.at (Harald Hofstätter), othmar@othmar-koch.org (Othmar Koch), michael.quell@yahoo.de (Michael Quell)

methods
2000 MSC: 65M20, 65M50, 65M70, 81-08

---

1. Introduction

We compare time integration methods for nonlinear Schrödinger equations of the type

$$\mathrm{i}\partial_t \psi(t) = A\psi(t) + B(\psi(t)) = H(\psi(t)), \quad \psi(0) = \psi_0, \tag{1.1}$$

on a Banach space $\mathscr{B}$. Here, $A : \mathscr{D} \subseteq \mathscr{B} \to \mathscr{B}$ is a self-adjoint differential operator and B a generally unbounded nonlinear operator.

Equations of this type commonly arise from model reductions of high-dimensional quantum dynamical systems serving to make quantum simulations computationally tractable. Examples of such model reductions are the Gross-Pitaevskii equation (GPE) for Bose-Einstein condensates (BEC) [1], which constitutes a meanfield theory for ultracold dilute bosonic gases, the multiconfigurational time-dependent Hartree for bosons (MCTDHB) method for ultracold bosonic atoms [2], the multiconfigurational time-dependent Hartree-Fock (MCTDHF) method [3, 4, 5] and its most current extension, the time-dependent complete-active-space self-consistent-field (TD-CASSCF) method for electron dynamics in atoms and small molecules [6], and time-dependent density functional theory (TDDFT) for extended systems such as large molecules, nanostructures and solid-state systems [7]. All of these ab initio methods imply (systems of) nonlinear Schrödinger equations for the orbitals which are highly sensitive to the accuracy of numerical integration, and whose propagation constitutes a major challenge.

Numerical discretization in space in the context of the method of lines gives rise to large systems of nonlinear ODEs. In the numerical time propagation, the number of operations per time step and the overall number of time steps can soon become prohibitive. In some applications, a significant speed-up will be critical for the feasibility of a simulation. A method which optimizes the time-steps with reliable error control is thus essential. In this way systems with larger numbers of particles will become tractable. A similar study of adaptivity within splitting methods has been conducted earlier for parabolic problems in [8].

Different approaches to the numerical solution of quantum dynamical systems have been discussed in the literature. While for the ab initio solution of the linear two-particle Schrödinger equation the short iterative Lanczos algorithm has

proven to be very efficient [9], it is not suitable for nonlinear orbital equations especially in the presence of strong nonlinearity. Often Runge-Kutta algorithms are used within multiconfigurational methods because of their robustness and broad applicability [6, 10]. Other splitting methods than those proposed below have been used, e.g., in [11] where the orbital equations of motion are split from the equations of motion for the configuration amplitudes and a matrix exponentiation algorithm is applied.

Adaptive time-splitting methods promise advantages both with respect to the computational effort in each time step and with respect to the number of required time-steps to achieve a prescribed accuracy. The underlying idea of adaptive time-splitting methods is the following: Time-splitting methods are based on multiplicative combinations of the partial flows of the vector fields, where the coefficients in this composition are determined such that a prescribed order of consistency is obtained [12]. Quantum systems and the associated reduced model equations comprise two or more vector fields of different stiffness. If these are treated separately, the resulting subproblems can typically be integrated with more efficient schemes. For instance, for the cubic nonlinear Schrödinger equation, the kinetic part can be integrated efficiently after (pseudo)spectral space discretization by exponentiation of a diagonal matrix, while the nonlinear part allows an exact integration of the resulting ordinary differential equations in real space. Thus, the numerical effort effectively reduces to transformations between real and frequency space, which can be implemented with low cost also in a parallel environment by fast transforms like fast Fourier transform (FFT), sine transform, etc. In contrast, explicit finite difference methods like Runge–Kutta or linear multistep methods typically suffer from instabilities unless time-steps are very small, while implicit methods like Crank-Nicholson have attractive stability and conservation properties, but the computational effort for the solution of the nonlinear equations is a serious drawback. The benefits of splitting methods as compared to competing time integrators have been extensively discussed in the mathematics literature in recent years. A comprehensive overview of recent investigations of splitting and finite difference methods for BEC is given in [13], which summarizes most of the studies conducted in this field. It turns out that the Crank-Nicholson finite difference method preserves most invariants like reversibility, mass and energy conservation and it is unconditionally stable. However, the computational cost for this fully implicit method is considerable, and the conservation properties only hold up to the accuracy of the nonlinear solver. Semi-implicit relaxation methods which only treat the linear term implicitly share the conservation properties if only a cubic nonlinearity is present and the kinetic part is treated implicitly,

but they are still computationally expensive and suffer from stability limitations. Semi-implicit finite difference schemes lose most of the desired properties. Time-splitting methods in conjunction with (pseudo)spectral methods (either based on Fourier or Sine bases) are overall concluded to be the most successful discretization schemes in the presence of smooth solutions. They are unconditionally stable, conserve norm, a (modified) energy functional and dispersion, which is not the case for many other time-stepping schemes. The spectral accuracy of the space discretization is only advantageous in the presence of regular solutions, however. For unsmooth or random spatial profiles, splitting methods in conjunction with finite difference spatial discretizations may be more efficient (see [14]). Finite element spatial discretizations, which are among the most popular and successful methods for problems on finite (irregular) domains where the solutions suggest to realize spatial adaptivity, are not the first choice in our context, as typically spatial adaptivity is less important than spectral accuracy. Extensive numerical comparisons in the literature additionally confirm the accuracy and efficiency of splitting methods for various quantum mechanical models under a number of different spatial discretizations. In an earlier work [15] it was concluded that a split-step Fourier method performs best overall for a number of test problems, and in [16] that time-splitting in conjunction with different spatial discretizations is most accurate and efficient and has desirable conservation properties. Recent improvements of this approach are given by non-uniform spectral spatial discretizations realized via non-uniform fast Fourier transforms (NUFFT), which can account for spatial variations in the problem smoothness [17, 18, 19]. The particular situation of highly oscillatory Schrödinger equations has recently been given special attention in the works [20, 21]. The potential advantages of splitting into more than two operators, which will also be briefly discussed in the present paper, are investigated in [22] for a magnetic Schrödinger equation, where a convergence proof is indicated for a first-order splitting into three operators, and in [23], which introduces four-operator splittings of order up to four with real or complex coefficients applied to the semiclassical Schrödinger equation. Overall, the theoretical and experimental evidence for the superior performance of time-splitting methods, which are usually used in conjunction with (pseudo)spectral space discretizations, is overwhelming in the mathematical literature.

The efficiency of the time-discretization can be improved if high-order time propagators are employed. Adaptive choice of the time-steps promises a further reduction in the computational effort. To provide a solid basis for such an approach, a theoretical analysis of the error structure is essential. A rigorous mathematical error analysis of splitting methods was first given in [24] for low

order methods applied to linear Schrödinger equations. An extension to higher-order schemes is provided by [25]. The nonlinear setting was first analyzed for the second-order Strang splitting in [26], and a convergence proof for high-order methods which also covers the cubic nonlinear Schrödinger equation and the equations of motion associated with MCTDHF is given in [4]. Theoretical error bounds for rotating BEC by a Fourier–Laguerre–Hermite splitting method are given in [27], while fully implicit finite difference methods are analyzed in [28]. An alternative theoretical framework for the analysis of splitting methods based on the defect of the numerical solution was recently developed in [29] for linear problems and also extended to the nonlinear case in [30]. The convergence was analyzed for evolution equations of Schrödinger type. This also includes the construction and theoretical analysis of a posteriori error estimators for the purpose of designing adaptive schemes. The defect-based approach, which is described in Section 3.2, is a universally applicable alternative to more special constructions based on embedded pairs of schemes [31], see Section 3.1. The latter are challenging to construct since a large system of nonlinear algebraic equations has to be solved, but the resulting schemes are cheaper to realize for high-order splitting methods. Another class of error estimates we consider are based on the property of the splitting coefficients being palindromic (Section 3.3).

Based on the local error estimates, successful time-stepping strategies can be implemented. To ensure a stable and efficient procedure, state-of-the-art step-size choice is based on firm theoretical ground by recent investigations based on digital filters from signal processing and control theory, see [32]. These methods have also been demonstrated to enhance computational stability [33] and have the potential to provide advantages for critical computations. We have observed some benefits in the presence of wave chaos in example (4.3), see Section 5.

To assess the applicability and efficiency of our numerical methods, we will resort to a number of low-dimensional model problems which are representative of the encountered structure, however. These comprise the cubic nonlinear Schrödinger equation [34], the Gross–Pitaevskii equation for a rotating Bose–Einstein condensate [14] and under a highly oscillatory potential [35], a two-component system modelling the propagation of pulses with equal mean frequencies in birefringent nonlinear fibers [36], and a model of quantum control of atomic systems [37].

In the final Section 6, we will demonstrate the successful application of our methods to nonlinear wave equations, which serve as suitable models to demonstrate the contribution of adaptive step-size choice to computational stability near the limit imposed by a CFL condition (the Courant–Friedrichs–Levy condition

represents a limit of the time-step in terms of the spatial discretization parameter which is generally necessary for the stability of time integrators for hyperbolic evolution equations).

2. Splitting methods

At the (time-)semi-discrete level, s-stage exponential splitting methods for the integration of (1.1) use multiplicative combinations of the partial flows $\mathscr{E}_A(t,u)$: $u \mapsto u(t) = \mathrm{e}^{tA}u$ and $\mathscr{E}_B(t,u) : u \mapsto u(t)$ with $u'(t) = B(u(t)),\ u(0) = u$. For a single step $(0,u_0) \mapsto (h,u_1)$ with time-step $t = h$, this reads

$$u_1 := \mathscr{S}(h,u_0) = \mathscr{E}_B(b_s h,\cdot) \circ \mathscr{E}_A(a_s h,\cdot) \circ \ldots \circ \mathscr{E}_B(b_1 h,\cdot) \circ \mathscr{E}_A(a_1 h,u_0), \qquad (2.1)$$

where the coefficients a_j, b_j, $j = 1 \ldots s$ are determined according to the requirement that a prescribed order of consistency is obtained [12].

Splitting into three terms. Splitting into more than two operators, which has first been analyzed theoretically for linear Schrödinger equations in [38], can also be beneficial when this is suggested by the special structure of the right-hand side of (1.1). A particular situation which suggests such a splitting is the following: For a problem with time-dependent coefficients, where $A = A(t),\ B = B(t,\psi)$, the independent variable t may be frozen over certain substeps in order to obtain subproblems which can be solved effectively, see [39]. To this end the given problem is reformulated as an autonomous system, where t formally becomes a dependent variable. In this way such a problem fits into the general context of splitting methods and can be analyzed on the basis of the general abstract theory. We will discuss such a problem specified in Section 4.4. Finally, nonlinear terms which cannot be explicitly integrated, e.g. if products of unknowns are involved, can be treated in a similar way.

Collection of methods. We have compiled a webpage with the most successful splitting formulae from the literature and a large number of optimized methods we constructed at

`http://www.asc.tuwien.ac.at/~winfried/splitting/`

which we will furtheron refer to as [40]. We will refrain from explicitly stating splitting formulae here for brevity.

3. Local error estimators

In this section, we briefly describe three classes of local error estimators which serve as our basis for adaptive time-stepping here and which have different advantages depending on the context in which they are applied. *Embedded pairs of splitting formulae* have been introduced in [31] and are based on reusing a number of evaluations from the basic integrator. A *defect-based* error estimator has been proposed and analysed in [29, 30, 38, 41]. For *palindromic pairs of formulae*, an asymptotically correct error estimator can be computed at the same cost as for the basic method, see [42]. The employed error estimates are *asymptotically correct*, i.e., the deviation of the error estimator from the true error tends to zero faster than does the error.

3.1. Embedded formulae

In [31], pairs of splitting schemes of orders p and $p+1$ are specified. The idea is to select a controller $\bar{\mathscr{S}}$ of order $p+1$ and to construct a worker $\mathscr{S}$ of order p for which a maximal number of compositions coincide with those of the controller. To construct pairs offering an optimal balance between cost and accuracy, we fix a 'good' controller of order $p+1$ and wish to adjoin to it a 'good' worker of order p. Since the number of compositions $\bar{s}$ in the controller will be higher than the number of compositions s in the worker, we can select an optimal embedded worker $\mathscr{S}$ from a set of candidates obtained by flexible embedding, where the number of coinciding coefficients is not a priori fixed. The idea is expanded in detail in [42], where optimized methods are determined. In this paper, we will focus on the pair `Emb 4/3 AK p` of orders four and three.

3.2. Defect-based estimators

In [29, 30, 38, 41], asymptotically correct error estimators based on the defect

$$\mathscr{D}(t,u(t)) := \partial_t \mathscr{S}(t,u(t)) - A\mathscr{S}(t,u(t)) - B(\mathscr{S}(t,u(t)))$$

have been constructed and analysed. In order to construct an error estimator associated with a splitting method of order $p \geq 1$, an integral representation of the local error involving $\mathscr{D}$ is approximated by means of an Hermite quadrature formula. Due to the fact that the validity of the p-th order conditions ensures that the first $p-1$ derivatives of $\mathscr{D}$ vanish at $t=0$, this leads to a local error estimator involving a single evaluation of the defect,

$$\mathscr{P}(h,u) = \tfrac{1}{p+1}\, h\, \mathscr{D}(h,u) \approx \mathscr{L}(h,u)\,. \tag{3.1}$$

This device works generally for splittings of any order into an arbitrary number of operators if Fréchet derivatives of the flows are available, see [43] (the Fréchet derivative of $\mathscr{E}_A(t,u)$ with respect to the second argument is subsequently denoted by $\partial_2\mathscr{E}_A(t,u)$ and likewise for all other flows). Algorithmically, for a splitting with s compositions the defect $d = \mathscr{D}(h,u)$ can be computed simultaneously with the update of the solution u as follows:

$$
\begin{aligned}
&d = 0\\
&\textbf{for}\ \ k = 1:s\\
&\quad d = d + a_k A(u)\\
&\quad d = \partial_2\mathscr{E}_A(a_k h,u)\cdot d\\
&\quad u = \mathscr{E}_A(a_k h,u)\\
&\quad d = \partial_2\mathscr{E}_B(b_k h,u)\cdot d\\
&\quad u = \mathscr{E}_B(b_k h,u)\\
&\quad d = d + \begin{cases} b_k B(u), & k < s\\ (b_k - 1)B(u), & k = s \end{cases}\\
&\textbf{end}\\
&d = d - A(u)
\end{aligned}
$$

3.3. Palindromic formulae

Let $\mathscr{S}$ be a palindromic scheme of odd order p (in the sense of [42]). In this case, the leading error terms of $\mathscr{S}$ and its adjoint $\mathscr{S}^*$ are identical up to the factor -1. Therefore, the averaged additive scheme

$$\bar{\mathscr{S}}(h,u) = \tfrac{1}{2}\left(\mathscr{S}(h,u) + \mathscr{S}^*(h,u)\right) \tag{3.2}$$

is a method of order $p+1$,[1] and

$$\mathscr{S}(h,u) - \bar{\mathscr{S}}(h,u) = \tfrac{1}{2}\left(\mathscr{S}(h,u) - \mathscr{S}^*(h,u)\right)$$

provides an asymptotically correct local error estimate for $\mathscr{S}(h,u)$. In this case the additional effort for computing the local error estimate is identical with the effort for the worker $\mathscr{S}$ but not higher as is the case for embedded pairs. This principle is limited to palindromic splitting methods of odd order, however. Since the error estimator is easy to construct and evaluate in this case, in addition to the method `PP 3/4 A` of basic order 3, we also employ the pair `PP 5/6 A` of orders 5/6.

[1] For the simplest case of the Lie-Trotter scheme this has already been observed in [44].

3.4. Step-size selection

Based on a local error estimator, the step-size is adapted such that the tolerance is expected to be satisfied in the following step. If h_{old} denotes the current step-size, the next step-size h_{new} in an order p method is predicted as (see [45, 46])

$$h_{\text{new}} = h_{\text{old}} \cdot \min\left\{\alpha_{\max}, \max\left\{\alpha_{\min}, \alpha\left(\frac{\text{tol}}{\mathscr{P}(h_{\text{old}})}\right)^{\frac{1}{p+1}}\right\}\right\}, \tag{3.3}$$

where $\alpha = 0.9$, $\alpha_{\min} = 0.25$, $\alpha_{\max} = 4.0$, and $\mathscr{P}(h_{\text{old}})$ is an asymptotically correct estimator for the local error arising in the previous time-step. This simple strategy incorporates safety factors to avoid an oscillating and unstable behavior.

More elaborate strategies based on digital filters and control theory are put forward in [32, 33, 47, 48]. As one example, we will also test a strategy incorporating a longer history, namely, the two previous step-sizes h_{-1}, h_{-2}, and associated error estimates $\mathscr{P}(h_{-1})$, $\mathscr{P}(h_{-2})$ enter the formula for the calculation of the new step-size,

$$h = h_{-1} \cdot \min\left\{\alpha_{\max}, \max\left\{\alpha_{\min}, \alpha\left(\frac{\text{tol}}{\mathscr{P}(h_{-1})}\right)^{\frac{\beta_1}{p+1}}\left(\frac{\text{tol}}{\mathscr{P}(h_{-2})}\right)^{\frac{\beta_2}{p+1}}\left(\frac{h_{-1}}{h_{-2}}\right)^{-\alpha_1}\right\}\right\}, \tag{3.4}$$

again with $\alpha = 0.9,\ \alpha_{\min} = 0.25$, $\alpha_{\max} = 4.0$, and with $\beta_1 = \beta_2 = \alpha_1 = 0.25$.

3.5. Global error estimator

Once a local error estimate is available, it can also be used to compute an estimate for the global error accumulated in the course of the integration. The general, heuristic idea (defect integration) is due to [49], which can be adapted to the current context: We integrate the local error estimate using a simple auxiliary scheme resulting in the desired global error estimate in an efficient way, since only a cheap low-order method has to be applied twice in addition to the expensive high-order integrator.

Consider the computational grid $\{t_\nu,\ \nu = 0, 1, 2, \ldots\}$ chosen either a priori or in an adaptive way, with time-steps $h_\nu = t_\nu - t_{\nu-1}$. The numerical solution values obtained are denoted by u_ν, and ε_ν denotes the global error estimate to be computed.

Along with the computed splitting approximation u_ν, we perform two simple integrations in parallel, e.g., using the Lie-Trotter scheme as an auxiliary integrator. Starting from $U_0 = \tilde{U}_0 = u_0$ we compute

$$U_\nu = \mathscr{S}_{aux}(t_{\nu-1}, U_{\nu-1}, h_\nu)\,, \tag{3.5a}$$

$$\tilde{U}_\nu = \mathscr{S}_{aux}(t_{\nu-1}, \tilde{U}_{\nu-1}, h_\nu) + \mathscr{P}(t_\nu, u_\nu)\,, \tag{3.5b}$$

for $\nu = 1, 2, \ldots$. Here, $\mathscr{S}_{aux}(t_{\nu-1}, \cdot, h_\nu)$ is the local flow of the auxiliary scheme, and $\mathscr{P}(t_\nu, u_\nu) \approx \mathscr{L}(t_\nu, u_\nu)$ denotes a local error estimate computed for the step $(t_{\nu-1}, u_{\nu-1}) \mapsto (t_\nu, u_\nu)$. Now we define the global error estimate as

$$\varepsilon_\nu = \tilde{U}_\nu - U_\nu\,, \quad \nu = 1, 2, \ldots \tag{3.6}$$

To motivate the design of this estimator, we note that by the definition of $\mathscr{L}(t_\nu, u_\nu) = \mathscr{S}(t_{\nu-1}, u_{\nu-1}, h_\nu) - \mathscr{E}_H(t_{\nu-1}, u_{\nu-1}, h_\nu)$ as the difference of two local flows, we have

$$u(t_\nu) = \mathscr{E}_H(t_{\nu-1}, u(t_{\nu-1}), h_\nu)\,, \tag{3.7a}$$
$$u_\nu = \mathscr{E}_H(t_{\nu-1}, u_{\nu-1}, h_\nu) + \mathscr{L}(t_\nu, u_\nu)\,, \tag{3.7b}$$

such that comparing (3.7) with (3.5) we may indeed expect

$$\varepsilon_\nu = \tilde{U}_\nu - U_\nu \approx u_\nu - u(t_\nu)\,, \quad \nu = 1, 2, \ldots \tag{3.8}$$

Evaluation of ε_ν is rather cheap, because the main effort lies in the evaluation of $\mathscr{P}(t_\nu, u_\nu)$ which is already available. ε_ν is propagated from $t_{\nu-1}$ to t_ν once u_ν has been accepted.

A further simplification is achieved by linearization, i.e., defining ε_ν by propagation of the linearized auxiliary scheme (with $\varepsilon_0 = 0$)

$$\varepsilon_\nu = \partial_2 \mathscr{S}_{\text{aux}}(t_{\nu-1}, u_{\nu-1}, h_\nu) \cdot \varepsilon_{\nu-1} + \mathscr{P}(t_\nu, u_\nu)\,, \quad \nu = 1, 2, \ldots, \tag{3.9}$$

where, e.g., for $\mathscr{S}_{\text{aux}} = \mathscr{S}_{\text{Lie}}$,

$$\begin{aligned}&\partial_2 \mathscr{S}_{\text{Lie}}(t_{\nu-1}, u_{\nu-1}, h_\nu)\\ &\quad = \partial_2 \mathscr{E}_B(t_{\nu-1}, \mathscr{E}_A(t_{\nu-1}, u_{\nu-1}, h_\nu), h_\nu) \cdot \partial_2 \mathscr{E}_A(t_{\nu-1}, u_{\nu-1}, h_\nu)\,.\end{aligned}$$

Here we do not give an analysis of the asymptotical correctness of this global error estimate. An example of its performance is included in Section 6.

4. Models from quantum dynamics

In this section, we give a number of test examples which are representative of the challenges encountered by high-order adaptive time integrators.

4.1. The cubic NLS

The cubic nonlinear Schrödinger equation [34] is given by

$$\mathrm{i}\,\partial_t \psi(x,t) = -\tfrac{1}{2}\Delta\psi(x,t) + \kappa\,|\psi(x,t)|^2\,\psi(x,t)\,, \tag{4.1a}$$

$$\psi(x,0) = \psi_0(x)\,, \qquad x \in \mathbb{R}^3\,, \quad t > 0\,, \tag{4.1b}$$

with $\kappa = -1$ and the initial condition chosen as

$$\psi(x) = \sum_{j=1}^{2} \frac{a_j\, e^{-ib_j x}}{\cosh(a_j(2x - c_j))}\,, \qquad x \in [-16, 16]\,, \tag{4.1c}$$

with $a_1 = a_2 = 2$, $b_1 = 1$, $b_2 = 3$, $c_1 = 5$, $c_2 = -5$. The cubic NLS has been treated earlier by our methods in [30], a theoretical analysis is given in [4]. The initial condition we prescribe here leads to a solution with two solitons which eventually cross [50], posing a challenge for an adaptive step-size selection algorithm and thus providing a serious benchmark for adaptive time-stepping, in contrast to the smoother solutions considered previously.

4.2. A two-component system

We consider a two-component system modelling the propagation of pulses with equal mean frequencies in birefringent nonlinear fibers [36],

$$\begin{aligned}
&\mathrm{i}\Big(\frac{\partial \psi_1}{\partial t} + \delta\frac{\partial \psi_1}{\partial x}\Big) + \frac{1}{2}\frac{\partial^2 \psi_1}{\partial x^2} + \big(|\psi_1|^2 + e\,|\psi_2|^2\big)\psi_1 = 0,\\
&\mathrm{i}\Big(\frac{\partial \psi_2}{\partial t} - \delta\frac{\partial \psi_2}{\partial x}\Big) + \frac{1}{2}\frac{\partial^2 \psi_2}{\partial x^2} + \big(e\,|\psi_1|^2 + |\psi_2|^2\big)\psi_2 = 0,
\end{aligned} \tag{4.2}$$

with exact solution (a pair of solitons)

$$\psi_1(x,t) = \frac{\sqrt{2\beta}}{1+e}\,\mathrm{sech}\big(\sqrt{2\beta}\,(x - vt)\big)\,\mathrm{e}^{\mathrm{i}\left((v-\delta)x + (\beta - (v^2-\delta^2)/2)t\right)},$$

$$\psi_2(x,t) = \frac{\sqrt{2\beta}}{1+e}\,\mathrm{sech}\big(\sqrt{2\beta}\,(x - vt)\big)\,\mathrm{e}^{\mathrm{i}\left((v+\delta)x + (\beta - (v^2-\delta^2)/2)t\right)},$$

which is exponentially decreasing with $|x|$. We start at $t = 0$, the parameters are chosen as $\delta = 0.5$, $\beta = 1.0$, $v = 1.1$, and $e = 0.8$. We impose periodic boundary conditions on the interval $[-50, 70]$. The problem has been solved by high-order splitting methods in [42].

4.3. The Gross–Pitaevskii equation with highly oscillatory potential

The Gross–Pitaevskii equation under a highly oscillatory potential inducing wave chaos is given for $x \in \mathbb{R}$ by

$$\mathrm{i}\,\partial_t \psi(x,t) = -\tfrac{1}{2}\Delta\psi(x,t) + V(x)\psi(x,t) + g|\psi(x,t)|^2\,\psi(x,t). \tag{4.3a}$$

The system parameters which are based on the experimental realization [2] lead to a rather large nonlinearity of $g \approx 400$ (in our implementation, we chose $g = 390$) in units of the harmonic trap in which the BEC is initially created. The initial condition

$$\psi(x,0) = \psi_0(x) \tag{4.3b}$$

is determined as the ground state of the harmonic oscillator, i.e. for $V(x) = \frac{1}{2}x^2$. For the initial state, see Figure 5.2. The harmonic trap is suddenly switched off, and at the same time a periodic potential $V(x) = v_0\cos(kx),\ v_0 = 1.4,\ k \approx 11.46$ is switched on in which the BEC then expands.

4.4. Quantum control

A model arising in quantum control of atomic systems which is discussed in [37] introduces a potential which explicitly depends on time:

$$i\,\partial_t \psi(x,t) = \varepsilon\Delta\psi(x,t) + \varepsilon^{-1}V(x,t)\,\psi(x,t)\,, \tag{4.4a}$$
$$\psi(x,0) = \psi_0(x)\,, \qquad x \in \mathbb{R}^3\,, \quad t > 0\,, \tag{4.4b}$$

with $V(x,t)$ and the initial condition chosen as:

$$\begin{aligned}
\psi_0(x) &= (\delta\pi)^{-\frac{1}{4}} e^{\frac{ik_0(x-x_0)}{\delta} - \frac{(x-x_0)^2}{2\delta}} \\
V(x,t) &= V_0(x) + \rho(3t-1)\rho(\sin(2\pi(x-t))) \\
V_0(x) &= \rho(4x)\sin(20\pi x) \\
\rho(x) &= \begin{cases} e^{\frac{-1}{1-x^2}}, & |x| < 1 \\ 0, & \text{otherwise,} \end{cases}
\end{aligned}$$

where $x_0 = -0.3,\ k_0 = 0.1,\ \delta = 10^{-3}$ and $\varepsilon = 2^{-8}$. With these parameters the initial condition is

$$\psi(x,0) = (10^{-3}\,\pi)^{-1/4}\,\mathrm{e}^{100\mathrm{i}(x+0.3) - 500\,(x+0.3)^2}, \tag{4.4c}$$

and the system is closed by periodic boundary conditions on $[-1,1]$.

4.5. Rotational Gross–Pitaevski equation

The Gross–Pitaevskii equation for a rotational Bose–Einstein condensate [14] is given by

$$\mathrm{i}\,\partial_t \psi(\mathbf{x},t) = \big(-\tfrac{1}{2}\Delta + V_{\mathrm{ext}}(\mathbf{x}) - \Omega L_z + \beta\,\big|\psi(\mathbf{x},t)\big|^2\big)\,\psi(\mathbf{x},t)\,, \tag{4.5a}$$

subject to asymptotic boundary conditions on the unbounded domain and an initial condition. For the sake of computation time, we consider the problem in two dimensions only, $\mathbf{x} = (x,y)$. $V_{\mathrm{ext}} : \mathbb{R}^2 \to \mathbb{R}$ denotes an external real-valued potential, which we assume to comprise a scaled harmonic potential that is symmetric with respect to the (x,y)-components and an additional sufficiently regular potential $V : \mathbb{R}^2 \to \mathbb{R}$

$$V_{\mathrm{ext}}(x) = \tfrac{1}{2}\,\gamma(x^2+y^2) + V(x)\,, \quad \gamma > 0\,. \tag{4.5b}$$

The rotation term involves the angular momentum rotation speed $\Omega \in \mathbb{R}$ and the angular momentum operator

$$L_z = -\mathrm{i}\,\big(x\,\partial_y - y\,\partial_x\big)\,. \tag{4.5c}$$

Besides, we denote by $\beta \in \mathbb{R}$ the interaction constant arising in the cubic nonlinearity. The parameters are chosen as

$$\gamma = 0.8\,, \quad \Omega = 0.5\,, \quad \beta = 100\,, \tag{4.5d}$$

$$\psi(x,y,0) = \tfrac{1}{\sqrt{\pi}}\,(x+\mathrm{i}\,y)\,\mathrm{e}^{-\frac{1}{2}(x^2+y^2)}\,, \quad (x,y) \in \mathbb{R}^2\,. \tag{4.5e}$$

This problem has first been solved by a Fourier–Laguerre–Hermite spectral method in [51], see also [52]. This allows to pose the asymptotically correct boundary conditions on the full space. Moreover, this example was solved in [53] under (artificial) periodic boundary conditions allowing a highly efficient dimensional splitting into three operators, see also [14]. In [54] this problem is treated by the Crank-Nicolson method, which we do not consider in our present comparison of adaptive splitting methods.

5. Numerical comparisons

Now we compare the performance of the most promising splitting methods in conjunction with some of the introduced error estimation and step selection methods for the models in Section 4. Runtime was measured throughout on an Intel Xeon E5-2670 with 8 cores, with the exception of problem (4.5), where computations were carried through on the Vienna Scientific Cluster.

5.1. Splitting into two operators

Cubic Schrödinger equation (4.1). We first compare the performance of different splitting methods for the cubic Schrödinger equation (4.1). We compare the computational effort for the methods `Emb 4/3 AK p`, `PP 3/4 A` of order 3 and `PP 5/6 A` of order 5, endowed with an asymptotically correct error estimator, respectively. This is given from the construction of the palindromic pairs or embedding idea, but additionally we use each integrator in conjunction with the defect-based error estimator. We use an underlying space discretization with $N = 1024$ Fourier modes in one spatial dimension.

It was found that the method with the least computational effort per step is `PP 3/4 A`, where 10000 equidistant steps required 1.37 seconds for the integrator and 2.73 seconds with the error estimator. For the other methods, 2.29 seconds / 3.19 seconds were measured for `Emb 4/3 AK p` and 3.68 / 7.07 seconds for `PP 5/6 A`, see Table 5.1.

Method	10000 steps	10000 steps with estimator
`Emb 4/3 AK p`	2.286	3.190
`PP 3/4 A`	1.370	2.731
`PP 5/6 A`	3.679	7.074
`Emb 4/3 AK p (defect)`	2.290	5.788
`PP 3/4 A (defect)`	1.633	3.583
`PP 5/6 A (defect)`	3.806	7.687

Table 5.1: Comparison of the computation costs of `Emb 4/3 AK p`, `PP 3/4 A`, and `PP 5/6 A` for (4.1).

In an adaptive setting, the higher order however pays off when a strict tolerance is prescribed, for tolerances 10^{-8} and 10^{-10} the method `PP 5/6 A` was the fastest, only for the mildest requirement of 10^{-5} the other methods proved competitive. `PP 5/6 A` provided the fastest integration, and adaptive step-size selection is more efficient in each case. The reason is obviously the challenging solution dynamics when the solitons cross, as there the adaptively chosen step-size drops abruptly. The comparison here and also for the other examples below is with respect to an equidistant grid based on the smallest step-size that the adaptive algorithm generated. We observe furthermore that the defect-based error estimator is invariantly more expensive than the palindromic pairs in each step, but recall that this is applicable in conjunction with any splitting scheme. Still, for the methods of orders 3/4, the embedding approach proved more efficient, which can be attributed to a smaller leading error term of the integrator, see the local error measures of 0.06 versus 00.25 listed at [40]. The results are given in Table 5.2.

There and later in the paper, the columns give the number of steps '# adapt' required to reach the prescribed tolerance in an adaptive computation, '# equidist' the number of equidistant steps required to achieve the same accuracy, and the time in seconds 'time adapt' respectively 'time equidist' the computations took in the two settings, respectively. The step-sizes generated by the adaptive procedure based on the method `PP 5/6 A` are shown in Figure 5.1. The drop in the step-size is clearly visible at the time where the solitons cross.

Method	# adapt	# equidist	time adapt	time equidist
`Emb 4/3 AK p`, TOL = 10^{-5}	275	1070	0.140	0.322
`PP 3/4 A`, TOL = 10^{-5}	438	1749	0.186	0.333
`PP 5/6 A`, TOL = 10^{-5}	156	501	0.167	0.240
`Emb 4/3 AK p (defect)`, TOL = 10^{-5}	265	1034	0.159	0.261
`PP 3/4 A (defect)`, TOL = 10^{-5}	438	1749	0.187	0.305
`PP 5/6 A (defect)`, TOL = 10^{-5}	189	733	0.203	0.350
`Emb 4/3 AK p`, TOL = 10^{-8}	1536	6005	0.716	1.654
`PP 3/4 A`, TOL = 10^{-8}	2478	9900	0.924	1.606
`PP 5/6 A`, TOL = 10^{-8}	504	2005	0.494	0.901
`Emb 4/3 AK p (defect)`, TOL = 10^{-8}	1495	5847	0.845	1.401
`PP 3/4 A (defect)`, TOL = 10^{-8}	2478	9900	0.993	1.648
`PP 5/6 A (defect)`, TOL = 10^{-8}	567	2240	0.606	1.015
`Emb 4/3 AK p`, TOL = 10^{-10}	4854	18986	2.092	5.034
`PP 3/4 A`, TOL = 10^{-10}	7837	31311	3.025	5.005
`PP 5/6 A`, TOL = 10^{-10}	1136	4515	1.074	2.072
`Emb 4/3 AK p (defect)`, TOL = 10^{-10}	4728	18492	2.531	4.270
`PP 3/4 A (defect)`, TOL = 10^{-10}	7837	31311	3.003	5.100
`PP 5/6 A (defect)`, TOL = 10^{-10}	1174	4653	1.194	2.047

Table 5.2: Comparison of the efficiency of `Emb 4/3 AK p`, `PP 3/4 A`, and `PP 5/6 A` for (4.1) using the step-size selection algorithm (3.3). The tolerances were 10^{-5} (top), 10^{-8} (middle) and 10^{-10} (bottom), respectively.

For this example, we also assess the refined step adaptation strategy (3.4). The results are given in Table 5.3. We observe that in this situation, the strategy does not provide an advantage in most of the cases.

Coupled Schrödinger equations (4.2). We now compare our adaptive splitting schemes when applied to (4.2). As expected, the comparison of the computational effort (runtime in seconds) of our methods when applied to the coupled Schrödinger equations (4.2) for 1000 equidistant steps gives the same picture as for (4.1), `PP 3/4 A` is cheapest, and application of the error estimator roughly doubles the computation time, see Table 5.4. Throughout, we use an underlying space discretization with $N = 1024$ Fourier modes in one spatial dimension.

In an adaptive setting, we observe in Table 5.5 that nonuniform time grids provide an advantage in computational effort which ranges between a factor 1.5

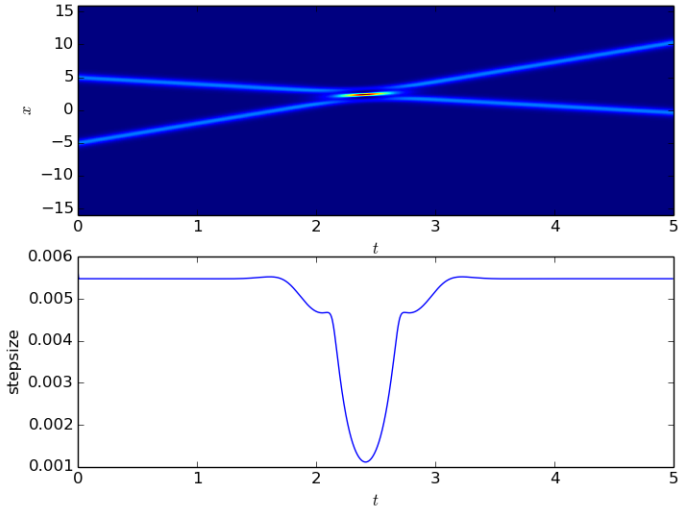

Figure 5.1: Solution of (4.1) (top), and step-sizes generated by an adaptive procedure based on `PP 5/6 A` with tolerance 10^{-10} (bottom).

Method	# adapt	# equidist	time adapt	time equidist
`Emb 4/3 AK p`, TOL = 10^{-5}	313	1218	0.140	0.291
`PP 3/4 A`, TOL = 10^{-5}	487	1945	0.177	0.300
`PP 5/6 A`, TOL = 10^{-5}	168	528	0.166	0.223
`Emb 4/3 AK p (defect)`, TOL = 10^{-5}	294	1148	0.153	0.260
`PP 3/4 A (defect)`, TOL = 10^{-5}	487	1945	0.162	0.269
`PP 5/6 A (defect)`, TOL = 10^{-5}	210	815	0.213	0.317
`Emb 4/3 AK p`, TOL = 10^{-8}	1751	6850	0.643	1.456
`PP 3/4 A`, TOL = 10^{-8}	2753	11000	0.959	1.778
`PP 5/6 A`, TOL = 10^{-8}	565	2251	0.540	1.017
`Emb 4/3 AK p (defect)`, TOL = 10^{-8}	1661	6497	0.905	1.515
`PP 3/4 A (defect)`, TOL = 10^{-8}	2753	11000	1.046	1.767
`PP 5/6 A (defect)`, TOL = 10^{-8}	626	2472	0.629	1.111
`Emb 4/3 AK p`, TOL = 10^{-10}	5536	21659	2.341	4.941
`PP 3/4 A`, TOL = 10^{-10}	8707	34790	2.890	5.642
`PP 5/6 A`, TOL = 10^{-10}	1265	5028	1.658	2.258
`Emb 4/3 AK p (defect)`, TOL = 10^{-10}	5252	20547	2.600	4.179
`PP 3/4 A (defect)`, TOL = 10^{-10}	8707	34790	3.053	5.325
`PP 5/6 A (defect)`, TOL = 10^{-10}	1300	5154	1.196	2.009

Table 5.3: Comparison of the efficiency of `Emb 4/3 AK p`, `PP 3/4 A`, and `PP 5/6 A` for (4.1), using the step-size selection algorithm (3.4). The tolerances were 10^{-5} (top), 10^{-8} (middle) and 10^{-10} (bottom), respectively.

and 4, with a significantly reduced number of steps, and a clear advantage for the

Method	10000 steps	10000 steps with estimator
`Emb 4/3 AK p`	17.70	32.47
`PP 3/4 A`	11.17	23.39
`PP 5/6 A`	19.67	45.64

Table 5.4: Comparison of the costs of `Emb 4/3 AK p`, `PP 3/4 A`, and `PP 5/6 A` for (4.2).

higher-order method for stricter tolerances. The alternative step-size choice (3.4) provides an advantage for this example only in half of the runs with the stricter tolerances, see Table 5.6.

Method	# steps adaptive	# steps equidist	time adaptive	time equidist
`Emb 4/3 AK p`, TOL = 10^{-5}	1034	5001	2.275	6.059
`PP 3/4 A`, TOL = 10^{-5}	1623	5087	2.601	4.863
`PP 5/6 A`, TOL = 10^{-5}	514	5001	3.225	14.765
`Emb 4/3 AK p`, TOL = 10^{-8}	5772	17733	16.955	26.519
`PP 3/4 A`, TOL = 10^{-8}	9200	28822	13.797	22.514
`PP 5/6 A`, TOL = 10^{-8}	1913	5909	11.671	17.438
`Emb 4/3 AK p`, TOL = 10^{-10}	18246	56065	42.758	65.400
`PP 3/4 A`, TOL = 10^{-10}	29100	91163	44.496	66.985
`PP 5/6 A`, TOL = 10^{-10}	4358	13372	18.216	26.749

Table 5.5: Comparison of the efficiency of `Emb 4/3 AK p`, `PP 3/4 A`, and `PP 5/6 A` for (4.2) using the step-size selection algorithm (3.3). The tolerances were 10^{-5} (top), 10^{-8} (middle) and 10^{-10} (bottom), respectively.

Method	# steps adaptive	# steps equidist	time adaptive	time equidist
`Emb 4/3 AK p`, TOL = 10^{-5}	1178	5001	2.471	5.837
`PP 3/4 A`, TOL = 10^{-5}	1806	5659	2.882	4.209
`PP 5/6 A`, TOL = 10^{-5}	582	5001	2.575	9.869
`Emb 4/3 AK p`, TOL = 10^{-8}	6583	20227	13.112	22.955
`PP 3/4 A`, TOL = 10^{-8}	10222	32026	17.924	26.983
`PP 5/6 A`, TOL = 10^{-8}	2154	6643	10.185	14.228
`Emb 4/3 AK p`, TOL = 10^{-10}	20813	63956	41.417	74.800
`PP 3/4 A`, TOL = 10^{-10}	32333	101293	50.280	73.950
`PP 5/6 A`, TOL = 10^{-10}	4856	14895	22.302	29.787

Table 5.6: Comparison of the efficiency of `Emb 4/3 AK p`, `PP 3/4 A`, and `PP 5/6 A` for (4.2), using the step selection algorithm (3.4). The tolerances were 10^{-5} (top), 10^{-8} (middle), and 10^{-10} (bottom), respectively.

Gross–Pitaevskii equation with periodic potential (4.3). The solution of the problem (4.3) is challenging for a numerical integrator due to the nonsmooth spatial

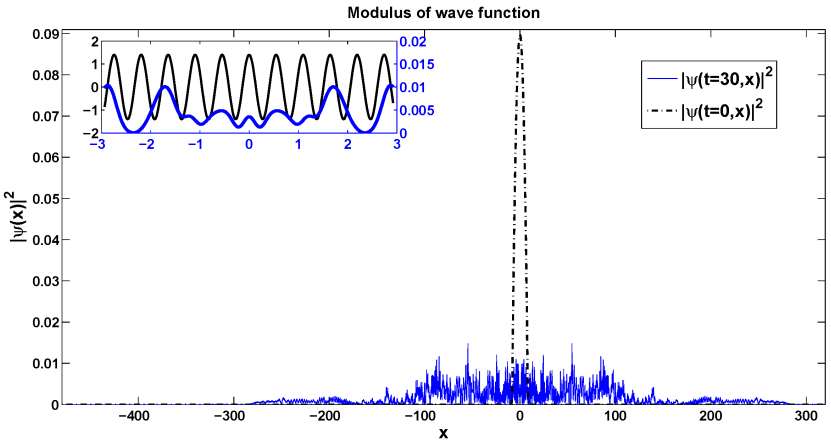

Figure 5.2: Squared modulus of the initial state and solution at $t = 30$ of (4.3). The inset displays the potential $V(x)$ (in black) whose amplitude is approximately one tenth of the mean particle energy, as well as a zoom of the non-smooth wavefunction at $t = 30$ (in blue).

solution profile. Wave chaos as measured by exponential divergence of two neighboring wave functions demonstrated for this system [35] provides a benchmark for speed and accuracy of the propagation algorithm. The non-smooth solution profile is illustrated in Figure 5.2 to give an indication of the numerical challenge. For this plot, we have chosen a Fourier spectral space discretization with 8196 basis functions on the interval $[-800, 800]$ and a sixth-order splitting method.

For the comparisons in Tables 5.8 and 5.9, we use an underlying space discretization with $N = 16384$ Fourier modes in one spatial dimension on $[-800, 800]$. Also for the Gross–Pitaevskii equation under a periodic potential (4.3), each splitting step is between two and three times more expensive when used in conjunction with an error estimator, see Table 5.7. Since this additional cost is not compensated for by a large variation in the time-steps, see Figure 5.3, the adaptive strategies are invariantly more expensive than uniform grids for this model. If adaptive time-stepping is used for reasons of reliability, it can be observed from Tables 5.8 and 5.9 that the defect-based error estimator is competitive with a palindromic pair, and higher-order methods are more efficient for strict tolerances. Most importantly, we observe that the step selection strategy (3.4) yields a more efficient method in the majority of tests for this example, which can most likely be attributed to the unsmooth solution dynamics. This contrasts the ambivalent picture observed in the other test problems.

Method	10000 steps	10000 steps with estimator
`Emb 4/3 AK p`	14.095	24.383
`PP 3/4 A`	9.938	27.758
`PP 5/6 A`	26.123	91.258
`Emb 4/3 AK p (defect)`	15.099	34.712
`PP 3/4 A (defect)`	9.810	22.504
`PP 5/6 A (defect)`	36.032	85.023

Table 5.7: Comparison of the costs of `Emb 4/3 AK p`, `PP 3/4 A`, and `PP 5/6 A` for (4.3).

Method	# steps adaptive	# steps equidist	time adaptive	time equidist
`Emb 4/3 AK p`, TOL = 10^{-5}	2233	2936	10.237	7.609
`PP 3/4 A`, TOL = 10^{-5}	3889	4204	14.029	7.299
`PP 5/6 A`, TOL = 10^{-5}	4368	4768	40.530	21.756
`Emb 4/3 AK p (defect)`, TOL = 10^{-5}	1984	2284	11.632	5.970
`PP 3/4 A (defect)`, TOL = 10^{-5}	3897	4207	15.152	7.306
`PP 5/6 A (defect)`, TOL = 10^{-5}	4363	4903	43.352	22.546
`Emb 4/3 AK p`, TOL = 10^{-8}	10598	11502	43.464	26.826
`PP 3/4 A`, TOL = 10^{-8}	21925	23743	67.694	36.652
`PP 5/6 A`, TOL = 10^{-8}	4282	4974	38.602	21.775
`Emb 4/3 AK p (defect)`, TOL = 10^{-8}	10356	11220	53.308	25.901
`PP 3/4 A (defect)`, TOL = 10^{-8}	21925	23745	70.223	23.364
`PP 5/6 A (defect)`, TOL = 10^{-8}	4365	5112	43.612	23.705
`Emb 4/3 AK p`, TOL = 10^{-10}	33518	36434	108.992	71.035
`PP 3/4 A`, TOL = 10^{-10}	69339	75092	188.785	113.936
`PP 5/6 A`, TOL = 10^{-10}	9326	10907	80.606	40.795
`Emb 4/3 AK p (defect)`, TOL = 10^{-10}	32656	35511	115.140	77.685
`PP 3/4 A (defect)`, TOL = 10^{-10}	69339	75093	181.419	94.820
`PP 5/6 A (defect)`, TOL = 10^{-10}	9367	10958	67.552	29.917

Table 5.8: Comparison of the efficiency of `Emb 4/3 AK p`, `PP 3/4 A`, and `PP 5/6 A` for (4.3) using the step-size selection algorithm (3.3). The tolerances were 10^{-5} (top), 10^{-8} (middle), and 10^{-10} (bottom), respectively.

Quantum control (4.4). When comparing our splitting methods when applied to (4.4), we observe a similar picture as for the other problems; the computational effort per time-step is the least for the palindromic pair `PP 3/4 A` and highest for `PP 5/6 A`, with `Emb 4/3 AK p` in between. In each case the error estimator roughly doubles the effort, see Table 5.10. In terms of efficiency, the higher-order method excels also for this problem, but adaptive step-size selection does not provide an advantage. Obviously, the variation in the solution is so fast and local that adaptive time-stepping cannot be exploited to increase the efficiency because the overall variation in the magnitude of step-sizes is moderate, see Figures 5.4 and in particular 5.5. Tables 5.11 and 5.12 give the computation times for simulations with the choices of the semiclassical parameter $\varepsilon = 2^{-8}$ and $\varepsilon = 10^{-5}$. The

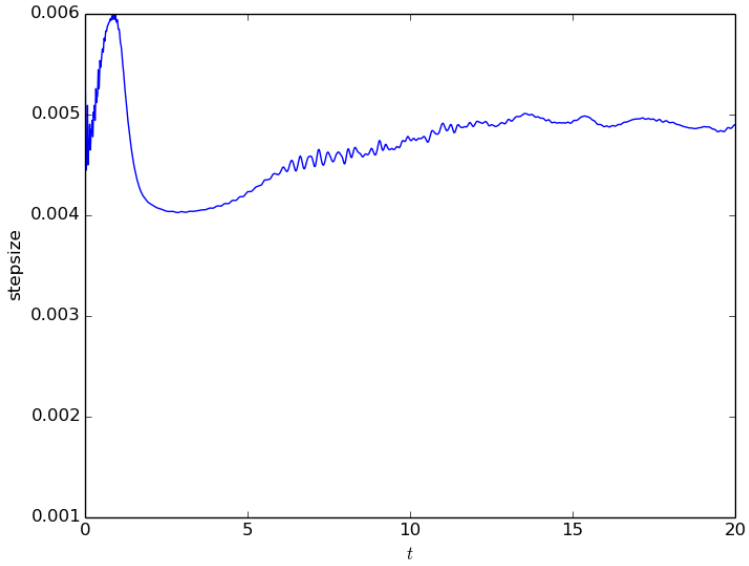

Figure 5.3: Step-sizes generated by an adaptive procedure based on `PP 5/6 A` with tolerance 10^{-8} for (4.3).

Method	# steps adaptive	# steps equidist	time adaptive	time equidist
`Emb 4/3 AK p`, TOL = 10^{-5}	2509	3796	10.895	9.196
`PP 3/4 A`, TOL = 10^{-5}	4323	4675	14.983	7.814
`PP 5/6 A`, TOL = 10^{-5}	4208	4662	37.393	20.366
`Emb 4/3 AK p (defect)`, TOL = 10^{-5}	2170	2362	12.039	5.886
`PP 3/4 A (defect)`, TOL = 10^{-5}	4323	4676	16.250	7.806
`PP 5/6 A (defect)`, TOL = 10^{-5}	2651	3272	26.262	14.704
`Emb 4/3 AK p`, TOL = 10^{-8}	12090	13100	48.395	30.010
`PP 3/4 A`, TOL = 10^{-8}	24360	26382	77.424	40.832
`PP 5/6 A`, TOL = 10^{-8}	4768	5547	42.373	19.359
`Emb 4/3 AK p (defect)`, TOL = 10^{-8}	11499	12436	37.963	23.752
`PP 3/4 A (defect)`, TOL = 10^{-8}	24361	26383	63.305	26.146
`PP 5/6 A (defect)`, TOL = 10^{-8}	4845	5674	31.079	16.623
`Emb 4/3 AK p`, TOL = 10^{-10}	38235	41474	95.876	57.318
`PP 3/4 A`, TOL = 10^{-10}	77042	83436	192.838	81.267
`PP 5/6 A`, TOL = 10^{-10}	10369	12132	56.940	32.112
`Emb 4/3 AK p (defect)`, TOL = 10^{-10}	36281	39352	114.484	63.763
`PP 3/4 A (defect)`, TOL = 10^{-10}	77042	83437	192.684	97.340
`PP 5/6 A (defect)`, TOL = 10^{-10}	10404	12172	94.398	52.434

Table 5.9: Comparison of the efficiency of `Emb 4/3 AK p`, `PP 3/4 A`, and `PP 5/6 A` for (4.3), using the step selection algorithm (3.4). The tolerances were 10^{-5} (top), 10^{-8} (middle) and 10^{-10} (bottom), respectively.

high-order method PP 5/6 A is the most efficient.

Method	10000 steps	10000 steps with estimator
Emb 4/3 AK p	43.955	76.494
PP 3/4 A	30.236	60.637
PP 5/6 A	80.363	161.206
Emb 4/3 AK p (defect)	44.012	93.266
PP 3/4 A (defect)	30.326	65.534
PP 5/6 A (defect)	80.574	166.907

Table 5.10: Comparison of the costs of Emb 4/3 AK p, PP 3/4 A, and PP 5/6 A for (4.4).

Method	# steps adaptive	# steps equidist	time adaptive	time equidist
Emb 4/3 AK p, TOL = 10^{-5}	117	139	0.905	0.608
PP 3/4 A, TOL = 10^{-5}	236	279	1.428	0.832
PP 5/6 A, TOL = 10^{-5}	80	90	1.292	0.720
Emb 4/3 AK p (defect), TOL = 10^{-5}	118	136	1.108	0.596
PP 3/4 A (defect), TOL = 10^{-5}	237	279	1.546	0.831
PP 5/6 A (defect), TOL = 10^{-5}	81	90	1.352	0.722
Emb 4/3 AK p, TOL = 10^{-8}	654	774	4.898	3.296
PP 3/4 A, TOL = 10^{-8}	1335	1570	7.796	4.525
PP 5/6 A, TOL = 10^{-8}	278	318	4.450	2.513
Emb 4/3 AK p (defect), TOL = 10^{-8}	640	753	5.861	3.214
PP 3/4 A (defect), TOL = 10^{-8}	1335	1570	8.430	4.527
PP 5/6 A (defect), TOL = 10^{-8}	280	323	4.626	2.550
Emb 4/3 AK p, TOL = 10^{-10}	2068	2446	15.059	10.163
PP 3/4 A, TOL = 10^{-10}	4222	4963	23.945	13.894
PP 5/6 A, TOL = 10^{-10}	636	755	9.970	5.857
Emb 4/3 AK p (defect), TOL = 10^{-10}	2016	2382	17.929	9.906
PP 3/4 A (defect), TOL = 10^{-10}	4222	4963	25.954	13.887
PP 5/6 A (defect), TOL = 10^{-10}	639	759	10.363	5.888

Table 5.11: Comparison of the efficiency of Emb 4/3 AK p, PP 3/4 A, and PP 5/6 A for (4.4) with $\varepsilon = 2^{-8}$ using the step-size selection algorithm (3.3). The tolerances were 10^{-5} (top), 10^{-8} (middle) and 10^{-10} (bottom), respectively.

5.2. Splitting into three operators — the rotational GPE (4.5)

In this section, we do not only compare the effectiveness of adaptive step-size selection as compared to uniform meshes, but also the two approaches put forward in [51] and [53], respectively. That is to say, on the one hand we use a spectral discretization by Laguerre–Fourier basis functions and splitting into two operators [51], on the other hand we use a dimensional splitting into three operators [53] in conjunction with Fourier basis functions in both spatial directions. The advantage of being able to use FFT transformations in the latter case by far

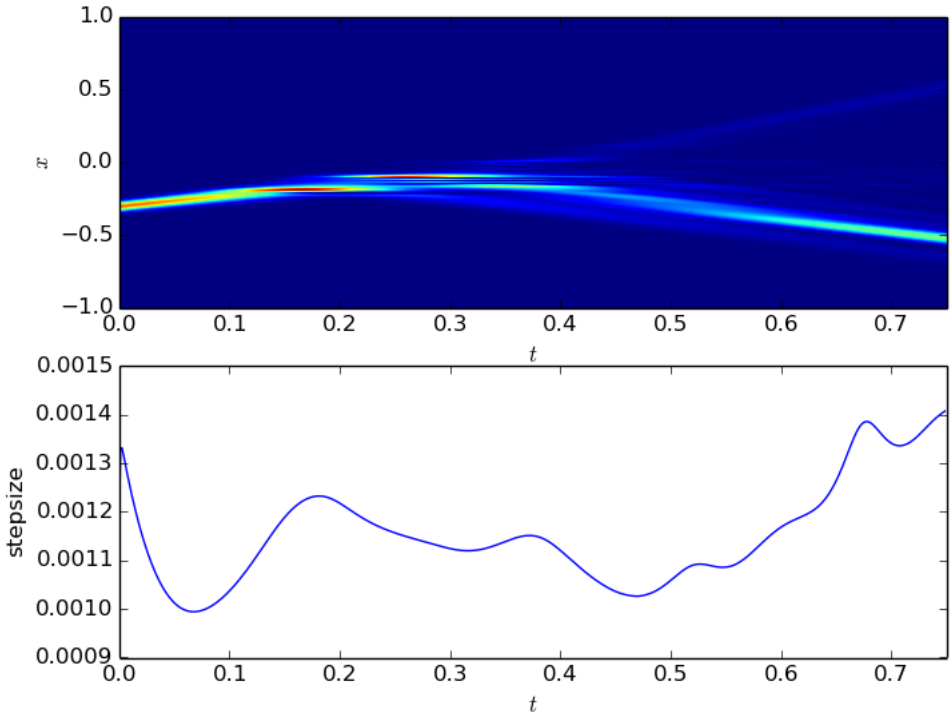

Figure 5.4: Solution (top) and step-sizes (bottom) generated for (4.4) with $\varepsilon = 2^{-8}$ for `PP 5/6 A` and tolerance 10^{-10}.

compensates for the increase in the number of compositions required for a higher-order *ABC*-splitting. It should be noted, however, that in this setting, artificial periodic boundary conditions have to be imposed in contrast to the asymptotically correct boundary treatment in the approach based on the generalized Laguerre functions. Both space discretizations use 250 basis functions in each of the two spatial directions.

The computations for the rotational GPE (4.5) were all performed on the Vienna Scientific cluster (VSC2). This consists of 1314 nodes, each with 2 processors (AMD Opteron 6132 HE, 2.2 GHz, 8 cores), that are interconnected via QDR InfiniBand. For our computations, one node (16 cores) was used.

From Table 5.13 we observe that use of the error estimator roughly doubles the computational effort in `Emb 4/3 AK p`, `PP 3/4 A`, and `PP 5/6 A` in both their original and defect-based versions, with significantly more effort for the highest-order method. The splitting into three operators `PP 3/4 A 3` is signifi-

Method	# steps adaptive	# steps equidist	time adaptive	time equidist
`Emb 4/3 AK p`, TOL = 10^{-5}	266	408	2.038	1.685
`PP 3/4 A`, TOL = 10^{-5}	454	715	2.906	1.998
`PP 5/6 A`, TOL = 10^{-5}	347	544	5.628	4.048
`Emb 4/3 AK p (defect)`, TOL = 10^{-5}	493	670	5.067	2.758
`PP 3/4 A (defect)`, TOL = 10^{-5}	695	1014	4.967	2.826
`PP 5/6 A (defect)`, TOL = 10^{-5}	591	801	9.886	5.954
`Emb 4/3 AK p`, TOL = 10^{-8}	3773	4909	26.776	19.825
`PP 3/4 A`, TOL = 10^{-8}	6792	9145	37.619	25.033
`PP 5/6 A`, TOL = 10^{-8}	2848	3660	42.256	26.909
`Emb 4/3 AK p (defect)`, TOL = 10^{-8}	3869	4845	34.049	19.576
`PP 3/4 A (defect)`, TOL = 10^{-8}	6806	9154	41.075	25.100
`PP 5/6 A (defect)`, TOL = 10^{-8}	3041	3764	46.953	27.618
`Emb 4/3 AK p`, TOL = 10^{-10}	10245	12986	71.741	52.214
`PP 3/4 A`, TOL = 10^{-10}	22123	29419	121.610	80.271
`PP 5/6 A`, TOL = 10^{-10}	6942	8489	101.739	61.931
`Emb 4/3 AK p (defect)`, TOL = 10^{-10}	9285	11614	80.047	46.714
`PP 3/4 A (defect)`, TOL = 10^{-10}	22126	29424	132.412	80.371
`PP 5/6 A (defect)`, TOL = 10^{-10}	6986	8519	106.526	62.276

Table 5.12: Comparison of the efficiency of `Emb 4/3 AK p`, `PP 3/4 A`, and `PP 5/6 A` for (4.4) with $\varepsilon = 10^{-5}$ using the step-size selection algorithm (3.3). The tolerances were 10^{-5} (top), 10^{-8} (middle) and 10^{-10} (bottom), respectively.

cantly cheaper to perform, and moreover the additional cost for the error estimator is lower here. The palindromic and the defect-based error estimators perform comparably.

Adaptive step-size choice yields an advantage in about half the cases, significantly so for two-operator splitting with the strictest tolerance, see Table 5.14. For the highest-order method `PP 5/6 A`, it was even impossible to finish the computation for the strictest tolerance in the time allotted on VSC. It is of greatest significance to observe that the three-operator splitting shows a tremendous computational advantage, which has to be contrasted however with the fact that in this case, artificial unphysical boundary conditions are imposed in contrast to the asymptotic boundary conditions in the Fourier–Laguerre approach.

The reason for the ambivalent picture obtained from the assessment of the merits of adaptive time-stepping for this example becomes clear if we look at the obtained step-sizes. The variation is rather moderate throughout the integration, it varies with some periodicity associated with the solution behavior over one or two orders of magnitude. Figure 5.6 shows the step-sizes for four different schemes, one embedded pair of methods and two palindromic pairs of orders 4 and 6, and a palindromic splitting into three operators. While the former generate comparable variations in the time-steps (of different sizes commensurate with the methods'

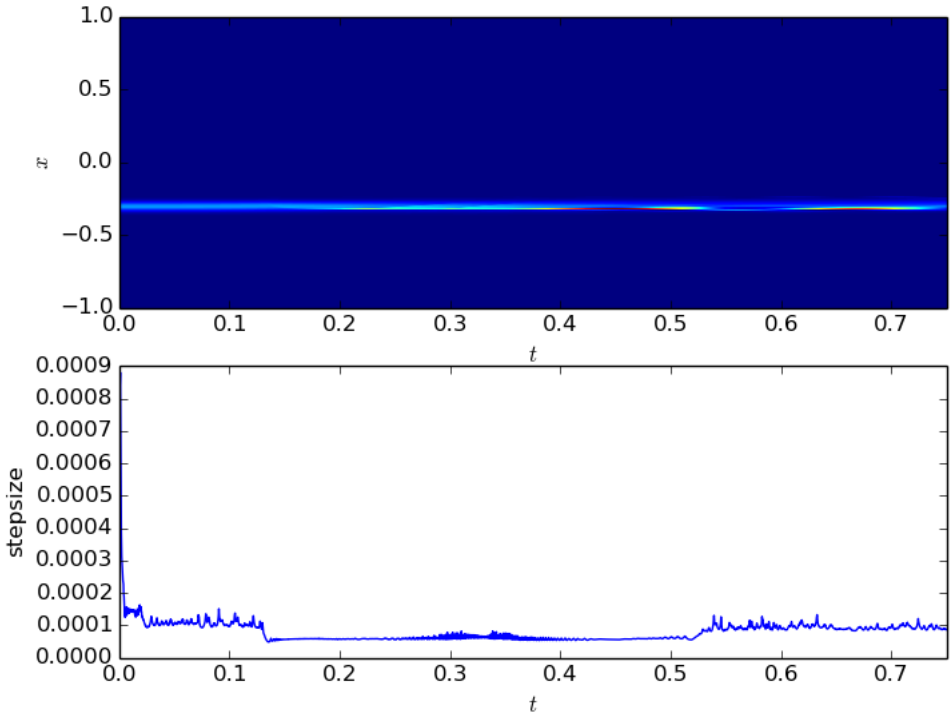

Figure 5.5: Solution (top) and step-sizes (bottom) generated for (4.4) with $\varepsilon = 10^{-5}$ for `PP 5/6 A` and tolerance 10^{-10}.

Method	1000 steps	1000 steps with estimator
`Emb 4/3 AK p`	764.991	1411.657
`PP 3/4 A`	623.102	1201.231
`PP 5/6 A`	1619.335	3224.533
`Emb 4/3 AK p (defect)`	837.905	2237.602
`PP 3/4 A (defect)`	604.044	1369.487
`PP 5/6 A (defect)`	1591.078	3414.450
`PP 3/4 A 3`	81.790	125.933
`PP 3/4 A 3 (defect)`	78.017	130.345

Table 5.13: Comparison of the costs of `Emb 4/3 AK p`, `PP 3/4 A` `PP 5/6 A`, and `PP 3/4 A 3` for (4.5).

accuracy), the latter displays quite different dynamics. This is to be attributed to the fact, that in the *ABC*-splitting, different operators are propagated which implies a quite different error behavior. This also accounts for the fact that the step-size variations are smaller.

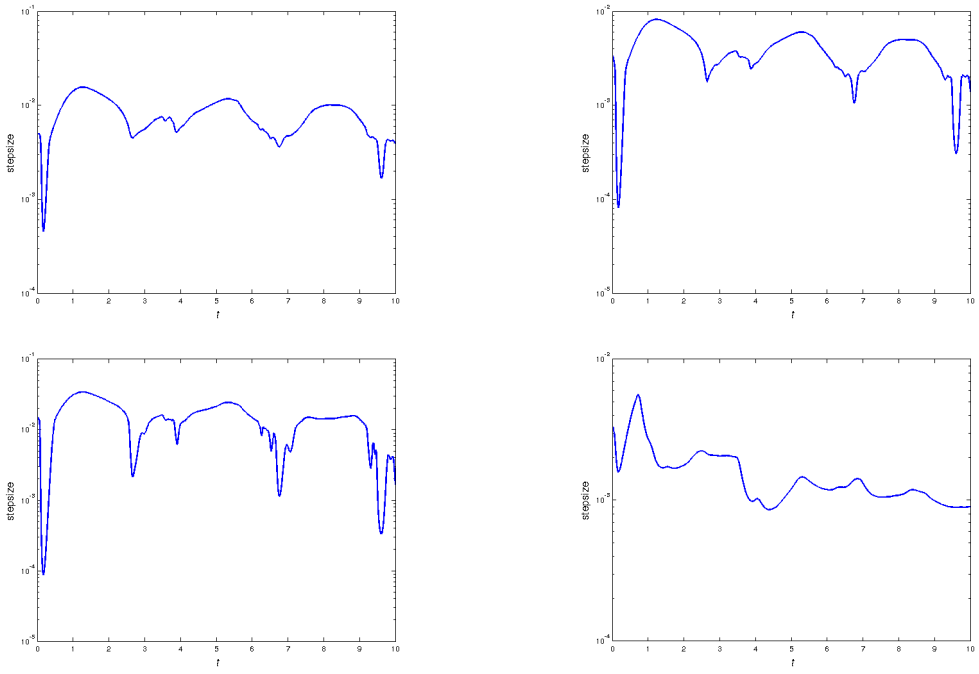

Figure 5.6: Step-sizes generated for (4.5) for the tolerance 10^{-8} for the methods `Emb 4/3 AK p` (top left), `PP 3/4 A` (top right), `PP 5/6 A` (bottom left), and `PP 3/4 A 3` (bottom right).

Method	# steps adaptive	# steps equidist	time adaptive	time equidist
`Emb 4/3 AK p`, TOL = 10^{-5}	257	593	331.750	453.639
`PP 3/4 A`, TOL = 10^{-5}	572	1199	698.655	747.099
`PP 5/6 A`, TOL = 10^{-5}	378	487	1294.096	788.616
`Emb 4/3 AK p (defect)`, TOL = 10^{-5}	292	656	692.364	549.665
`PP 3/4 A (defect)`, TOL = 10^{-5}	516	1160	725.644	700.69
`PP 5/6 A (defect)`, TOL = 10^{-5}	233	515	870.543	819.405
`PP 3/4 A 3`, TOL = 10^{-5}	1561	2379	242.647	194.578
`PP 3/4 A 3 (defect)`, TOL = 10^{-5}	1668	2601	216.260	202.922
`Emb 4/3 AK p`, TOL = 10^{-8}	1712	22151	2375.509	16945.315
`PP 3/4 A`, TOL = 10^{-8}	4844	124342	5983.282	77477.748
`PP 5/6 A`, TOL = 10^{-8}	2907	115357	9719.208	186801.627
`Emb 4/3 AK p (defect)`, TOL = 10^{-8}	1455	4950	3255.689	4147.629
`PP 3/4 A (defect)`, TOL = 10^{-8}	2940	6911	4201.668	4174.548
`PP 5/6 A (defect)`, TOL = 10^{-8}	870	7023	2970.675	11174.140
`PP 3/4 A 3`, TOL = 10^{-8}	7556	11701	1013.203	957.024
`PP 3/4 A 3 (defect)`, TOL = 10^{-8}	7832	12007	1030.912	936.750
`Emb 4/3 AK p`, TOL = 10^{-10}	50425	2211674	71295.689	1691910.704
`PP 3/4 A`, TOL = 10^{-10}	275133	12434140	327537.048	7747737.502
`PP 5/6 A`, TOL = 10^{-10}	−−	−−	−−	−−
`Emb 4/3 AK p (defect)`, TOL = 10^{-10}	5757	48767	12893.411	40862.113
`PP 3/4 A (defect)`, TOL = 10^{-10}	10035	55720	14202.577	33657.331
`PP 5/6 A (defect)`, TOL = 10^{-10}	5424	70839	18763.142	112710.374
`PP 3/4 A 3`, TOL = 10^{-10}	23510	36672	3136.493	2999.402
`PP 3/4 A 3 (defect)`, TOL = 10^{-10}	23659	36795	3145.173	2870.635

Table 5.14: Comparison of the efficiency of `Emb 4/3 AK p`, `PP 3/4 A`, `PP 5/6 A`, and `PP 3/4 A 3` for (4.5). The tolerances were 10^{-5} (top), 10^{-8} (middle) and 10^{-10} (bottom), respectively.

6. The Klein–Gordon equation

To conclude this study, we investigate hyperbolic nonlinear wave equations, since their solution is particularly sensitive to an appropriate choice of the time-steps which are required to satisfy a CFL (Courant–Friedrichs–Levi) condition (for hyperbolic problems, the time-step is commonly limited in terms of the spatial discretization parameter to ensure stability). We consider the Klein–Gordon equation endowed with periodic boundary conditions on the rectangular domain $[-32\pi, 32\pi]^2$,

$$\partial_{tt} u(x,y,t) = \Delta u(x,y,t) - u(x,y,t) + u^3(x,y,t), \tag{6.1a}$$
$$u(x,y,0) = u_0(x,y),\ u_t(x,y,0) = v_0(x,y). \tag{6.1b}$$

If we write this as a first order system

$$\partial_t u(x,y,t) = v(x,y,t), \tag{6.1c}$$
$$\partial_t v(x,y,t) = \Delta u(x,y,t) - u(x,y,t) + u^3(x,y,t), \tag{6.1d}$$

we can solve the problem by splitting into the vector fields

$$A := \begin{pmatrix} v \\ 0 \end{pmatrix}, \qquad B := \begin{pmatrix} 0 \\ \Delta u(x,y,t) - u(x,y,t) + u^3(x,y,t) \end{pmatrix}.$$

It turns out that for this partitioned system, splitting schemes are equivalent to partitioned Runge–Kutta methods, e.g. Strang splitting corresponds to the (symplectic) Störmer–Verlet method,

$$u_{j+1/2} = u_j + h/2\, v_j, \tag{6.2a}$$

$$v_{j+1} = v_j + h\,(u_{xx,j+1/2} - u_{j+1/2} + u^3_{j+1/2}), \tag{6.2b}$$

$$u_{j+1} = u_{j+1/2} + h/2\, v_{j+1}, \tag{6.2c}$$

where $u_{xx,j+1/2}$ is an approximation of the second spatial derivative computed from the entries of $u_{j+1/2}$.

Applying this second order scheme, we observe the expected empirical order three for the local error: We choose the domain $(x,y) \in [-32\pi, 32\pi]^2$ and impose periodic boundary conditions, as the initial condition we prescribe $u_0(x,y) = v_0(x,y) = \exp(-x^2 - y^2)$. The space discretization is based on a Fourier pseudospectral method on a grid with 512×512 points. In Table 6.1, ℓ_err gives the error with associated empirical order p_err, as computed with respect to a reference solution with timestep $1.22 \cdot 10^{-4}$, and δ_est and p_est refer to the deviation of the error estimator as compared to the true error (approximated via the reference solution). As expected, the error estimator is asymptotically correct, and the order three for the local error implies global order two, illustrated by g_err and p. Note that this check is performed here because for hyperbolic problems, no convergence theory of splitting methods is available.

h	ℓ_err	δ_est	p_err	p_est	g_err	p
5.000 E−01	0.309 E−03	0.242 E−03			0.219E-02	
2.500 E−01	0.280 E−04	0.163 E−04	3.46	3.89	0.226E-03	3.28
1.250 E−01	0.277 E−05	0.105 E−05	3.34	3.95	0.514E-04	2.13
6.250 E−02	0.299 E−06	0.667 E−07	3.21	3.98	0.126E-04	2.02
3.125 E−02	0.345 E−07	0.419 E−08	3.12	3.99	0.315E-05	2.01
1.563 E−02	0.414 E−08	0.261 E−09	3.06	4.01	0.787E-06	2.00
7.813 E−03	0.504 E−09	0.155 E−10	3.04	4.07	0.197E-06	2.00

Table 6.1: Empirical convergence orders of the local and the global errors for Strang splitting applied to the Klein–Gordon equation (6.1).

In the same setting, a symmetric fourth order composition method based on Strang splitting is applied to (6.1). In Table 6.2 we again observe the classical orders.

h	ℓ_err	δ_est	p_err	p_est	g_err	p
5.000 E−01	0.155E-02	0.149E-03			0.394E+00	
2.500 E−01	0.177E-04	0.154E-05	6.45	6.59	0.307E-01	3.68
1.250 E−01	0.220E-06	0.249E-07	6.33	5.95	0.115E-04	11.38
6.250 E−02	0.293E-08	0.408E-09	6.23	5.93	0.691E-06	4.06
3.125 E−02	0.706E-10	0.671E-11	5.37	5.93	0.427E-07	4.02
1.563 E−02	0.254E-11	0.111E-11	4.80	2.59	0.266E-08	4.00
7.813 E−03	0.884E-13	0.569E-12	4.85	0.97	0.166E-09	4.00
3.906 E−03	0.291E-14	0.287E-12	4.92	0.99	0.104E-10	4.00

Table 6.2: Empirical convergence orders of the local and the global errors for fourth order composition applied to the Klein–Gordon equation (6.1).

6.1. Defect evaluation

For the underlying problem class and solution method, the defect-based error estimate introduced in [30], see Section 3.2, can be implemented in a particularly simple way:

When a nonlinear wave equation of the form

$$\partial_{tt} u = \Delta u + f(u) \tag{6.3}$$

is rewritten as a system of first order as in (6.1), we obtain a partitioned system of the form

$$\begin{aligned} \partial_t u(t) &= G(v(t)), \\ \partial_t v(t) &= F(u(t)), \end{aligned} \tag{6.4}$$

where in our case G is the identity. This is solved by application of partitioned Runge-Kutta schemes which applied to (6.4) are equivalent to splitting schemes according to the splitting

$$\begin{pmatrix} \dot{u}(t) \\ \dot{v}(t) \end{pmatrix} = \begin{pmatrix} G(v(t)) \\ 0 \end{pmatrix} + \begin{pmatrix} 0 \\ F(u(t)) \end{pmatrix}. \tag{6.5}$$

In this special case, the defect-based local error estimator is particularly easy to specify and to evaluate, as explained in the following. Before discussing the general case, we give a detailed example to illustrate the argument.

Example: 2nd order partitioned Runge–Kutta scheme. Consider one step of a second order partitioned scheme (corresponding to Strang splitting), where

$(u_0, v_0) \mapsto (u(h), v(h))$:

$$u_1(h) = u_0 + \frac{h}{2} G(v_0), \tag{6.6a}$$
$$v(h) = v_0 + hF(u_1(h)), \tag{6.6b}$$
$$u(h) = u_1(h) + \frac{h}{2} G(v(h)). \tag{6.6c}$$

For evaluating the defect

$$\begin{pmatrix} \mathscr{D}_u \\ \mathscr{D}_v \end{pmatrix} = \begin{pmatrix} \dot{u}(h) - G(v(h)) \\ \dot{v}(h) - F(u(h)) \end{pmatrix} \tag{6.7}$$

of the numerical solution with respect to the given evolution equation (6.4), we consider h as continuous variable and differentiate equations (6.6):

$$\dot{u}_1(h) = \frac{1}{2} G(v_0), \tag{6.8a}$$
$$\dot{v}(h) = F(u_1(h)) + hF'(u_1(h)) \cdot \dot{u}_1(h) \tag{6.8b}$$
$$= F(u_1(h)) + hF'(u_1(h)) \cdot \frac{1}{2} G(v_0), \tag{6.8c}$$
$$\dot{u}(h) = \dot{u}_1(h) + \frac{1}{2} G(v(h)) + \frac{h}{2} G'(v(h)) \cdot \dot{v}(h). \tag{6.8d}$$

Hence,

$$\begin{aligned} \mathscr{D}_u(h) &= \dot{u}(h) - G(v(h)) \\ &= \dot{u}_1(h) + \frac{1}{2} G(v(h)) + \frac{h}{2} G'(v(h)) \cdot \dot{v}(h) - G(v(h)) \\ &= \frac{1}{2} \big(G(v_0) - G(v(h)) \big) + \frac{h}{2} G'(v(h)) \cdot \dot{v}(h), \end{aligned} \tag{6.9a}$$
$$\mathscr{D}_v(h) = \dot{v}(h) - F(u(h)). \tag{6.9b}$$

This can be realized algorithmically as follows:

$$\begin{aligned} w_1 &= \frac{1}{2} G(v_0), \\ w_2 &= \frac{1}{2} G(v(h)), \\ w_3 &= F(u_1(h)), \\ w_4 &= F(u(h)), \\ w_5 &= F'(u_1(h)) \cdot w_1, \\ w_6 &= w_3 + t\, w_5 \quad (= \dot{V}(h)), \\ w_7 &= G'(v(h)) \cdot w_6. \end{aligned}$$

Then,

$$\begin{aligned} \mathscr{D}_u &= w_1 - w_2 + \frac{h}{2} w_7, \\ \mathscr{D}_v &= w_6 - w_4. \end{aligned}$$

Taylor expansion immediately shows $\mathscr{D}_u = \mathscr{O}(h^2)$, $\mathscr{D}_v = \mathscr{O}(h^2)$. Thus,

$$\frac{h}{3} \mathscr{D} = \frac{h}{3} \begin{pmatrix} \mathscr{D}_u \\ \mathscr{D}_v \end{pmatrix} \tag{6.10}$$

is an estimate for the local error which is $\mathscr{O}(h^3)$; its deviation from the local error is $\mathscr{O}(h^4)$.

Next, we generalize this idea to higher-order splitting methods, which for convenience are constructed as (symmetric) compositions of Strang splitting substeps [12]. The general idea is the same as in [30]: For computing the defect, evaluations of the type $F'(u) \cdot w$ and $G'(v) \cdot w$ are required. We suppress the argument t. Let a_j, b_j denote the coefficients of the scheme. Starting at u_0, v_0 we have, for $j = 1 \ldots s$:

$$\begin{aligned} u_j &= u_{j-1} + h a_j G(v_{j-1}) =: \phi(h, u_{j-1}, v_{j-1}), \\ v_j &= v_{j-1} + h b_j F(u_j) =: \psi(h, u_j, v_{j-1}). \end{aligned} \tag{6.11}$$

Then, $u(h) = u_s$, $v(h) = v_s$.

For evaluating the defect $(\mathscr{D}_u, \mathscr{D}_v)$ of $(u(h), v(h))$ with respect to the given evolution equation (6.4), we use a recursion for the evaluation of the derivatives of the intermediate approximations: Starting at $\dot{u}_0 = \dot{v}_0 = 0$ we have for $j = 1 \ldots s$:

$$\begin{aligned} \dot{u}_j &= \dot{u}_{j-1} + a_j \left(G(v_{j-1}) + h G'(v_{j-1}) \dot{v}_{j-1} \right) =: \Phi(t, \dot{u}_{j-1}, v_{j-1}, \dot{v}_{j-1}), \\ \dot{v}_j &= \dot{v}_{j-1} + b_j \left(F(u_j) + h F'(u_j) \dot{u}_j \right)) =: \Psi(h, u_j, \dot{u}_j, \dot{v}_{j-1}). \end{aligned} \tag{6.12}$$

With $u = u_s, v = v_s, \dot{u} = \dot{u}_s, \dot{v} = \dot{v}_s$, this finally yields the defect

$$\mathscr{D} = \begin{pmatrix} \mathscr{D}_u \\ \mathscr{D}_v \end{pmatrix} = \begin{pmatrix} \dot{u} - G(v) \\ \dot{v} - F(u) \end{pmatrix}.$$

If the scheme has order p, the local error estimate is now given by

$$\frac{h}{p+1}\,\mathscr{D}, \tag{6.13}$$

and its deviation from the exact local error is $\mathscr{O}(h^{p+2})$.

6.2. Adaptive time-stepping

To illustrate the robustness of adaptive time-stepping we consider the Strang splitting (realized as above) applied to (6.1), with an underlying space discretization of 512×512 Fourier modes on $[-32\pi, 32\pi]^2$. If we apply adaptive time-stepping relying on the defect-based error estimator (Section 3.2) to satisfy a tolerance of $= 10^{-5}$, we obtain the time-steps displayed in Figure 6.1.

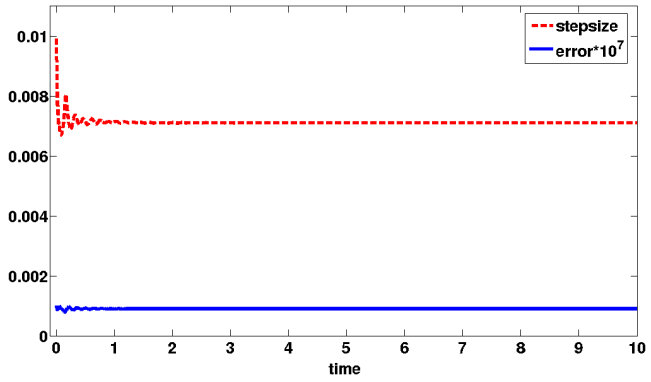

Figure 6.1: Adaptive time-stepping and local error for (6.1).

6.3. 1D illustrations

To illustrate the behavior of our adaptive time-stepping strategy further, we consider two examples for wave equations in one spatial dimension where exact solutions and their properties are known.

Klein–Gordon equation. First, we consider (6.1) for $x \in [-50, 50]$, with an underlying Fourier pseudospectral discretization at $N = 4096$ points. The solution is computed by the Strang splitting according to (6.6).

The initial condition for (6.1) is chosen such as to yield the exact (soliton) solution

$$u(x,t) = \sqrt{2}\,\operatorname{sech}\left(\frac{x-ct}{\sqrt{1-c^2}}\right), \qquad c = 0.5,$$

which is known to be orbitally unstable (implying solution blowup under small perturbations, see [55]). Our adaptive time-stepping method correctly diagnoses this behavior and consistently enforces $\Delta t \to 0$ as the solution approaches blow-up. Figure 6.2 shows the generated time-steps when a tolerance of 10^{-9} is imposed.

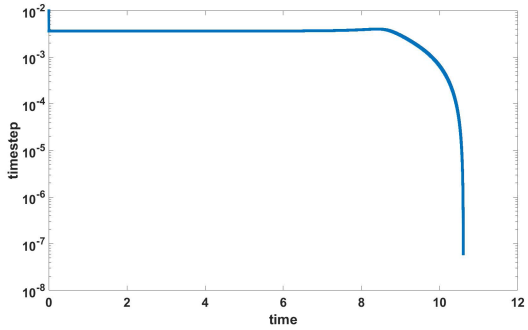

Figure 6.2: Adaptive time-stepping for (6.1) for orbitally unstable 1D soliton.

Sine–Gordon equation. We solve the Sine–Gordon equation

$$\partial_{tt} u(x,t) \;=\; \Delta u(x,t) - \sin(u(x,t)), \qquad u(x,0) = u_0(x),\ u_t(x,0) = v_0(x), \tag{6.14a}$$

where the initial condition is chosen such that the exact solution is the so-called *breather solution*

$$u(x,t) = 4\arctan\left(\frac{\tan(2)\cos\left(\gamma\cos(2)(t-0.1x)\right)}{\cosh\left(\gamma\sin(2)(x-0.1t)\right)}\right). \tag{6.14b}$$

We integrate in time on $[0, 20]$ and observe that the time-steps are consistent with the variation of the smoothness of the oscillating solution.

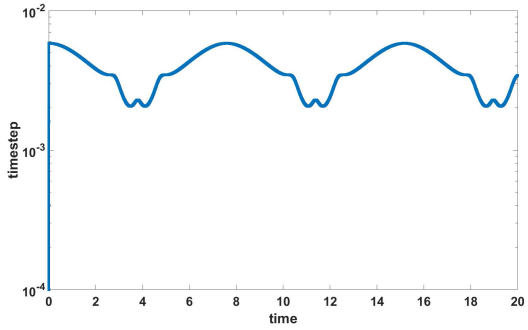

Figure 6.3: Adaptive time-stepping for Strang applied to (6.14) with breather solution.

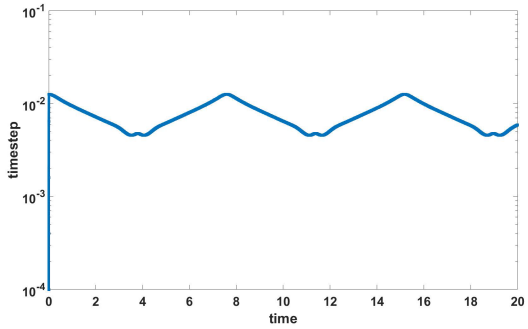

Figure 6.4: Adaptive time-stepping for [40, `Emb 4/3 AK p`] applied to (6.14) with breather solution.

Figure 6.3 shows the time-steps chosen for the Strang splitting (6.2) with an underlying tolerance of 10^{-12}, and likewise for the fourth-order method [40, `Emb 4/3 AK p`], see Figure 6.4.

To additionally illustrate the reliability of our error control, we also apply our global error estimate from Section 3.5 in the linearized version (3.9) and monitor the energy[2] conservation for (6.14). We integrate for $t \in [0,20]$ with the second order Strang splitting and with the fourth order composition, respectively. If a tolerance of 10^{-9} is prescribed for the second order method, the maximum of the

[2]The total energy for the Sine–Gordon equation is defined by the integral $\int_{-50}^{50} \left(\frac{1}{2}(\partial_t u)^2 + \frac{1}{2}(\partial_x u)^2 - \cos(u)\right) dx$.

error in the two components is $1.95 \cdot 10^{-5}$, while the deviation of the global error estimator from the true error is $4.02 \cdot 10^{-7}$. The energy difference between the initial state and the approximation at $t = 20$ is $4.78 \cdot 10^{-8}$. For the fourth order composition with a tolerance 10^{-12}, we observe a global error of $5.52 \cdot 10^{-9}$ and a deviation of $7.27 \cdot 10^{-11}$. The energy difference here is $2.48 \cdot 10^{-12}$. All these observations of the numerical errors are consistent with a reliable error control steering the solution process at the prescribed tolerance if we recall that the global error results from the accumulation of local errors.

Stability. It is well known that explicit Runge–Kutta type methods are required to satisfy a CFL condition (step-size limitation in relation to the spatial discretization parameter, see [56]) for a stable integration of hyperbolic problems. This is also observed for splitting methods, which is in particular clear in the cases where we have shown above that these are equivalent. We see that if in our adaptive procedure the tolerance is chosen as too large, the numerical solution may satisfy the error tolerance, but violate the CFL condition. This leads to numerical instability. While adaptive step-size choice correctly diagnoses this behavior and reduces the time-step accordingly, this still leads to an undesirably inefficient computation due to the large number of rejected time-steps. In Figure 6.5 we observe such a behavior when the last computation for (6.14) (see Figure 6.4) is repeated with a tolerance 10^{-6} instead of 10^{-9}. Indeed, about 15% of the time-steps are rejected and the time-steps oscillate, indicating the location of the stability threshold. Still, the adaptive procedure achieves to compute a reliable solution with a global error $3.89 \cdot 10^{-4}$ at $T = 20$.

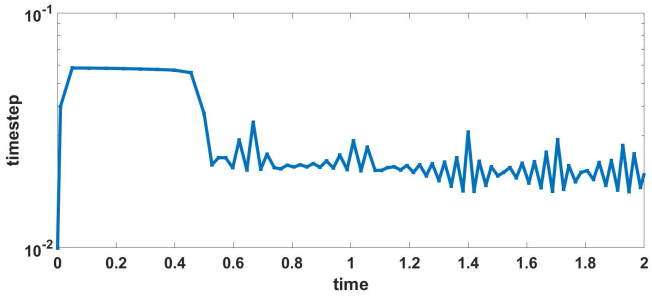

Figure 6.5: Step selection near the regime of instability for (6.14).

7. Conclusions

We have investigated adaptive time-stepping for splitting methods applied to nonlinear Schrödinger equations representative for the challenges encountered in problems arising in large-scale simulations of quantum dynamics. The problems comprise the cubic Schrödinger equation with focussing nonlinearity with the solution given by two crossing solitons, a two-component system, the Gross–Pitaevskii equation with a highly oscillatory potential triggering wave chaos, a problem representative for quantum control, and the rotational Gross–Pitaevskii equation. We have employed various splitting schemes of different orders and estimators for the time-stepping error and have compared their efficiency. It turned out that a significant advantage in computational efficiency is to be expected when the solution shows a singular critical event where the solution becomes unsmooth as in blowup or the crossing of solutions, whereas for rapidly varying solutions only with the strictest tolerances adaptivity may show an advantage. Among the different error estimators are pairs of methods with embedded coefficients, palindromic pairs of schemes, and defect-based error estimators. In most cases, higher-order methods perform favorably, where error estimators are most economically constructed for methods with palindromic coefficients. Generally, the biggest advantage of a time-adaptive strategy is revealed when no suitable initial guess for the appropriate step-size is available. Moreover, we have demonstrated for wave equations that adaptive step-size selection provides a tool for diagnosing and avoiding instability for instance induced by a CFL condition.

Acknowledgments

This work was supported by the Vienna Science and Technology Fund (WWTF) [grant number MA14-002] and the Austrian Science Fund (FWF) [grant number P24157-N13]. The computational results presented have been achieved in part using the Vienna Scientific Cluster (VSC).

References

[1] C. J. Pethick, H. Smith, Bose–Einstein Condensation in Dilute Gases, Cambridge University Press, Cambridge, 2008.

[2] O. Alon, A. Streltsov, L. Cederbaum, Multiconfigurational time-dependent Hartree method for bosons: Many-body dynamics of bosonic systems, Phys. Rev. A 77 (2008) 033613.

[3] T. Kato, H. Kono, Time-dependent multiconfiguration theory for electronic dynamics of molecules in an intense laser field, Chem. Phys. Lett. 392 (2004) 533–540.

[4] O. Koch, C. Neuhauser, M. Thalhammer, Error analysis of high-order splitting methods for nonlinear evolutionary Schrödinger equations and application to the MCTDHF equations in electron dynamics, M2AN Math. Model. Numer. Anal. 47 (2013) 1265–1284.

[5] J. Zanghellini, M. Kitzler, C. Fabian, T. Brabec, A. Scrinzi, An MCTDHF approach to multi-electron dynamics in laser fields, Laser Physics 13 (8) (2003) 1064–1068.

[6] T. Sato, K. L. Ishikawa, Time-dependent complete-active-space self-consistent-field method for multielectron dynamics in intense laser fields, Phys. Rev. A 88 (2013) 023402.

[7] C. A. Ullrich, Time-Dependent Density-Functional Theory: Concepts and Applications, Oxford University Press, Oxford; New York, 2011.

[8] W. Auzinger, O. Koch, M. Quell, Adaptive high-order splitting methods for systems of nonlinear evolution equations with periodic boundary conditions, Numer. Algorithms 75 (2017) 261–283.

[9] J. Feist, S. Nagele, R. Pazourek, E. Persson, B. I. Schneider, L. A. Collins, J. Burgdörfer, Nonsequential two-photon double ionization of helium, Phys. Rev. A 77 (2008) 043420.

[10] I. Březinová, A. U. J. Lode, A. I. Streltsov, O. E. Alon, L. S. Cederbaum, J. Burgdörfer, Wave chaos as signature for depletion of Bose–Einstein condensates, Phys. Rev. A 86 (2012) 013630.

[11] D. Haxton, K. Lawler, C. McCurdy, Multiconfiguration time-dependent Hartree-Fock treatment of electronic and nuclear dynamics in diatomic molecules, Phys. Rev. A 83 (2011) 063416.

[12] E. Hairer, C. Lubich, G. Wanner, Geometric Numerical Integration, Springer-Verlag, Berlin–Heidelberg–New York, 2002.

[13] X. Antoine, W. Bao, C. Besse, Computational methods for the dynamics of the nonlinear Schrödinger/Gross–Pitaevskii equations, Comput. Phys. Commun. 184 (2013) 2621–2633.

[14] W. Bao, Y. Cai, Mathematical theory and numerical methods for Bose–Einstein condensation, Kinet. Relat. Mod. 6 (2013) 1–135.

[15] Q. Chang, E. Jia, W. Sun, Difference schemes for solving the generalized nonlinear Schrödinger equation, J. Comput. Phys. 148 (1999) 397–415.

[16] W. Bao, Q. Tang, Z. Xu, Numerical methods and comparison for computing dark and bright solitons in the nonlinear Schrödinger equation, J. Comput. Phys. 235 (2013) 423–445.

[17] S. Jiang, L. Greengard, W. Bao, Fast and accurate evaluation of nonlocal Coulomb and dipole–dipole interactions via the nonuniform FFT, SIAM J. Sci. Comput. 36 (2014) B777–B794.

[18] W. Bao, S. Jiang, Q. Tang, Y. Zhang, Computing the ground state and dynamics of the nonlinear Schrödinger equation with nonlocal interactions via the nonuniform FFT, J. Comput. Phys. 296 (2015) 72–89.

[19] W. Bao, Q. Tang, Y. Zhang, Accurate and efficient numerical methods for computing ground states and dynamics of dipolar Bose–Einstein condensates via nonuniform FFT, Commun. Comput. Phys. 19 (2016) 1141–1166.

[20] P. Chartier, N. Mauser, F. Méhats, Y. Zhang, Solving highly-oscillatory nonlinear schrödinger equations with SAM: Numerical efficiency and geometric properties, Discrete and Continuous Dynamical Systems – Series S 9 (2016) 1327–1349.

[21] P. Chartier, F. Méhats, M. Thalhammer, Y. Zhang, Improved error estimates for splitting methods applied to highly-oscillatory nonlinear Schrödinger equations, Math. Comp. 85 (2016) 2863–2885.

[22] M. Caliari, A. Ostermann, C. Piazzola, A splitting approach for the magnetic Schrödinger equation, J. Comput. Appl. Math. 316 (2017) 74–85.

[23] P. Chartier, L. Le Treust, F. Méhats, Uniformly accurate methods for the semiclassical Schrödinger equation. Part 1: Construction of schemes and simulations, preprint available from `https://hal.archives-ouvertes.fr/hal-01140880v2`.

[24] T. Jahnke, C. Lubich, Error bounds for exponential operator splittings, BIT 40 (2000) 735–744.

[25] M. Thalhammer, Convergence analysis of high-order time-splitting pseudo-spectral methods for nonlinear Schrödinger equations, SIAM J. Numer. Anal. 50 (2012) 3231–3258.

[26] C. Lubich, On splitting methods for Schrödinger–Poisson and cubic nonlinear Schrödinger equations, Math. Comp. 77 (2008) 2141–2153.

[27] H. Hofstätter, O. Koch, M. Thalhammer, Convergence analysis of high-order time-splitting pseudo-spectral methods for rotational Gross-Pitaevskii equations, Numer. Math. 127 (2014) 315–364.

[28] W. Bao, Y. Cai, Optimal error estimates of finite difference methods for the Gross–Pitaevskii equation with angular momentum rotation, Math. Comp. 82 (2013) 99–128.

[29] W. Auzinger, O. Koch, M. Thalhammer, Defect-based local error estimators for splitting methods, with application to Schrödinger equations, Part II: Higher-order methods for linear problems, J. Comput. Appl. Math. 255 (2013) 384–403.

[30] W. Auzinger, H. Hofstätter, O. Koch, M. Thalhammer, Defect-based local error estimators for splitting methods, with application to Schrödinger equations, Part III: The nonlinear case, J. Comput. Appl. Math. 273 (2014) 182–204.

[31] O. Koch, C. Neuhauser, M. Thalhammer, Embedded split-step formulae for the time integration of nonlinear evolution equations, Appl. Numer. Math. 63 (2013) 14–24.

[32] G. Söderlind, Time-step selection algorithms: Adaptivity, control and signal processing, Appl. Numer. Math. 56 (2006) 488–502.

[33] G. Söderlind, L. Wang, Adaptive time-stepping and computational stability, J. Comput. Appl. Math. 185 (2006) 225–243.

[34] C. Sulem, P.-L. Sulem, The Nonlinear Schrödinger Equation, Appl. Math. Sciences, Springer-Verlag, New York, 1999.

[35] I. Březinová, L. Collins, K. Ludwig, B. Schneider, J. Burgdörfer, Wave chaos in the nonequilibrium dynamics of the Gross–Pitaevskii equation, Phys. Rev. A 83 (2011) 043611.

[36] M. Wadati, T. Iizuka, M. Hisakado, A coupled nonlinear Schrödinger equation and optical solitons, J. Phys. Soc. Jpn. 61 (1992) 2241–2245.

[37] A. Iserles, K. Kropielnicka, P. Singh, On the discretisation of the semiclassical Schrödinger equation with time-dependent potential, preprint, available from http://www.damtp.cam.ac.uk/user/na/NA_papers/NA2015_02.pdf.

[38] W. Auzinger, O. Koch, M. Thalhammer, Defect-based local error estimators for high-order splitting methods involving three linear operators, Numer. Algorithms 70 (2015) 61–91.

[39] S. Blanes, F. Casas, A. Farrés, J. Laskar, J. Makazaga, A. Murua, New families of symplectic splitting methods for numerical integration in dynamical astronomy, Appl. Numer. Math. 68 (2013) 58–72.

[40] W. Auzinger, O. Koch, Coefficients of various splitting methods, http://www.asc.tuwien.ac.at/~winfried/splitting/.

[41] W. Auzinger, O. Koch, M. Thalhammer, Defect-based local error estimators for splitting methods, with application to Schrödinger equations, Part I: The linear case, J. Comput. Appl. Math. 236 (2012) 2643–2659.

[42] W. Auzinger, H. Hofstätter, D. Ketcheson, O. Koch, Practical splitting methods for the adaptive integration of nonlinear evolution equations. Part I: Construction of optimized schemes and pairs of schemes, BIT 57 (2017) 55–74. doi:10.1007/s10543-016-0626-9.

[43] W. Auzinger, W. Herfort, Local error structures and order conditions in terms of Lie elements for exponential splitting schemes, Opuscula Math. 34 (2014) 243–255.

[44] G. Strang, On the construction and comparison of difference schemes, SIAM J. Numer. Anal. 5 (1968) 506–517.

[45] E. Hairer, S. Nørsett, G. Wanner, Solving Ordinary Differential Equations I, Springer-Verlag, Berlin–Heidelberg–New York, 1987.

[46] W. Press, B. Flannery, S. Teukolsky, W. Vetterling, Numerical Recipes in C — The Art of Scientific Computing, Cambridge University Press, Cambridge, U.K., 1988.

[47] G. Söderlind, Automatic control and adaptive time-stepping, Numer. Algorithms 31 (2002) 281–310.

[48] G. Söderlind, Digital filters in adaptive time-stepping, ACM Trans. Math. Software 29 (2003) 1–26.

[49] H. J. Stetter, The defect correction principle and discretization methods, Numer. Math. 29 (1978) 425–443.

[50] M. Ismail, T. Taha, Numerical simulation of coupled nonlinear Schrödinger equation, Math. Comput. Simulation 56 (2001) 547–562.

[51] W. Bao, J. Shen, A fourth-order time-splitting Laguerre–Hermite pseudospectral method for Bose–Einstein condensates, SIAM J. Sci. Comput. 26 (6) (2005) 2010–2028.

[52] W. Bao, H. Li, J. Shen, A generalized-Laguerre–Fourier–Hermite pseudospectral method for computing the dynamics of rotating Bose–Einstein condensates, SIAM J. Sci. Comput. 31 (5) (2009) 3685–3711. doi:10.1137/080739811.

[53] W. Bao, H. Wang, An efficient and spectrally accurate numerical method for computing dynamics of rotating Bose-Einstein condensates, J. Comput. Phys. 217 (2006) 612–626.

[54] W. Bao, Q. Du, Y. Zhang, Dynamics of rotating Bose–Einstein condensates and its efficient and accurate numerical computation, SIAM J. Appl. Math. 66 (2006) 758–786.

[55] R. Donninger, W. Schlag, Numerical study of the blowup/global existence dichotomy for the focusing cubic nonlinear Klein–Gordon equation, Nonlinearity 24 (2011) 2547–2562.

[56] J. Strikwerda, Finite Difference Schemes and Partial Differential Equations, Wadsworth & Brooks/Cole, Pacific Grove, 1989.